



UNITED NATIONS EDUCATIONAL, SCIENTIFIC AND CULTURAL ORGANIZATION  
INTERNATIONAL ATOMIC ENERGY AGENCY  
INTERNATIONAL CENTRE FOR THEORETICAL PHYSICS  
I.C.T.P., P.O. BOX 586, 34100 TRIESTE, ITALY. CABLE: CENTRATOM TRIESTE



H4.SMR/1013-37

**SCHOOL ON THE USE OF SYNCHROTRON RADIATION  
IN SCIENCE AND TECHNOLOGY:  
*"John Fuggle Memorial"***

**3 November - 5 December 1997**

***Miramare - Trieste, Italy***

---

***Dynamical Theory of X-ray Diffraction by Perfect Crystals***

**H. Tolentino  
National Laboratory for Synchrotron Radiation (LNLS)  
Campinas, Brazil**

Lecture

“Dynamical theory of X-ray Diffraction  
by perfect crystals”

by Hélio Tolentino

# Dynamical Theory of X-ray Diffraction

## by Perfect Crystals

deals with the propagation of waves in a periodic structure in a self-consistent way; couples the incident and diffracted waves

successive stages of accounting for the physical phenomena

### geometrical theory

directions under which diffracted rays appear.

### kinematical theory

combined effect of wavelets in directions other than those of maximum cooperation is taken into account; diffracted amplitudes are negligible compared to incident amplitude.

no attenuation -> energy is not conserved

good for thin crystals & imperfect crystals

### dynamical theory

find conditions for a wave field exist and travel through the perfect crystal; connect fields inside the crystal to those outside.

-> solving **Maxwell equations in a Perfect Periodic system**

... quantum & relativistic effects ...

### historical

1912/13 Friedrich, Knipping and Laue discovered X-ray diffraction

*Annalen der Physik*, **41**, 971 (1913)

1913 Bragg relation  $n\lambda = 2d \sin \theta$

*Proc. Camb.Phil.Soc.*, **17**, 43 (1913)

1914 Darwin : interaction of each atom in the structure with the incident wave, neglecting its interaction with the scattered waves. Good for structural crystallography; bad for diffracted intensities

*Phil.Mag.*, **27**, 315 (1914) (I); **27**, 675 (1914) (II)

1916/17 Ewald : the crystal is formed by a tridimensional array of point resonators (oscilating dipoles) responsible for scattering of the electromagnetic field.

*Annalen der Physik*, **49**, 1 and 117 (1916); **54**, 519 (1917)

1931 Laue : consider a continuum electron density distribution, described by a dielectric constant - periodic and complex, similar to Bethe's developpment for electron diffraction

*Ergeb. exakt.Naturwiss.*, **10**, 133 (1931)

### Bibliography

B. W. Batterman and R. Cole, Rev. of Modern Physics, 36-3, 681 (1964)

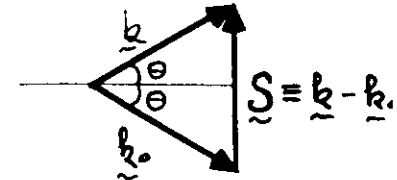
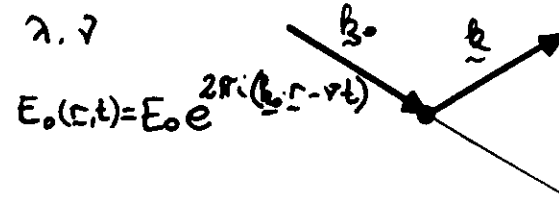
R.W. James, "The Optical Principles of the Diffraction of X-rays", Ox Bow Press (Woodbridge, Connecticut, USA - 1982)

W.H. Zachariasen, "Theory of X-ray Diffraction in Crystals", John Wiley (New York, USA - 1945)

J. Baruchel, J.L. Hodeau, M.S. Lehmann, J.R. Regnard and C. Schlenker, "Neutron and Synchrotron Radiation for Condensed Matter Studies", Springer-Verlag/Les editions de Physique (Les Ulis, France - 1993)

### X-ray Diffraction

o scattering from electrons in an atom



free electron  $\underline{E}_e = -\frac{e^2}{mc^2} \frac{E_0(r,t)}{R}$

(3)

$|\underline{k}_0| = \frac{1}{\lambda} = |\underline{k}|$

Thomson scattering

electrons in an atom (far from any resonance)

$$\frac{E_{\text{rad}}}{E_e} = f(s) = \int \rho(r) e^{2\pi i \vec{s} \cdot \vec{r}} d^3r$$

for  $s=0$   $f(0) = \int \rho(r) d^3r = Z$

bound electrons in an atom (resonance and absorption)

$$E_e = -\frac{e^2}{mc^2} \frac{E_0(r,t)}{R} \cdot \frac{\omega_0^2}{\omega_0^2 - \omega^2 - i\gamma\omega_0}$$

$$\Rightarrow f(s) = f_0(s) + f' + i f''$$

o periodic structure - perfect crystal ( $\underline{a}$ ,  $\underline{b}$ ,  $\underline{c}$ )

$$\rho(\underline{r}) = \frac{1}{V} \sum_{\underline{h}} F_{\underline{h}} e^{-2\pi i \underline{h} \cdot \underline{r}}$$

$\underline{h}$  must be a reciprocal lattice vector:  $\underline{h} = h \underline{a}^* + k \underline{b}^* + l \underline{c}^*$   
to ensure that  $\rho(\underline{r}) = \rho(\underline{r} + u \underline{a} + v \underline{b} + w \underline{c})$

$$F_{\underline{h}} = \int_{cell} \rho(\underline{r}) e^{2\pi i \underline{h} \cdot \underline{r}} dV$$

within the assumption that the atoms behave as rigid spheres with respect to their charges densities and are not vibrating thermally

$$F_{\underline{h}} = \sum_n f_n e^{2\pi i \underline{h} \cdot \underline{r}_n}$$

the structure factor is the 'sum' of the scattering factor of each atom in the unit cell.  $\underline{r}_n$  is the vector fixing the center of each atom.

$$f_n \rightarrow f_n e^{-M_n} \quad \text{Debye-Waller factor}$$

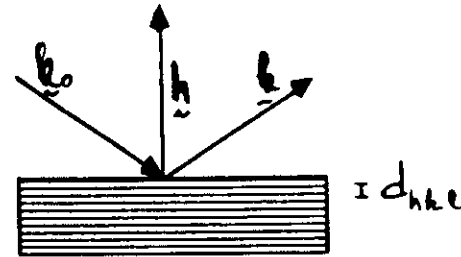
$$Si \text{ and } Ge: M_n = \frac{6h^2 T}{m k_B} \left( 1 + \left( \frac{\theta}{6T} \right)^2 \right) \left( \frac{1}{2} \leq \right)^2$$

Bathrow and Chiprow (1962)

$$\underline{S} = \underline{k} - \underline{k}_0 = \underline{h} \quad \text{or} \quad \underline{S} \cdot \underline{a} = \underline{h}, \text{ etc...}$$

Laue conditions

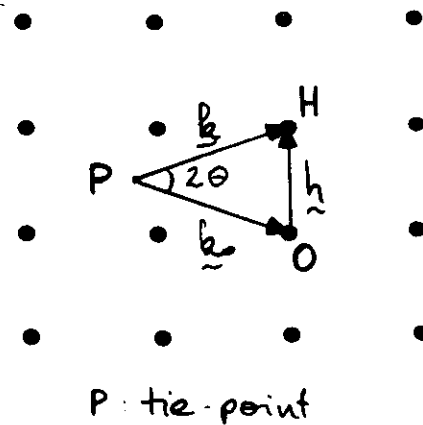
two useful properties of  $\underline{h}$ :  
i)  $\underline{h}$  is perpendicular to hkl plans  
ii)  $|\underline{h}| = 1/d_{hkl}$



the positions of the nodes in the reciprocal lattice give the periodicity of  $\rho(\underline{r})$ , hence of the crystal

### Ewald's construction

reciprocal lattice



$$\frac{|\underline{h}|}{2} = |\underline{k}| \sin \theta = |\underline{k}_0| \sin \theta$$

$$\frac{1}{\lambda} \sin \theta = \frac{1}{d_{hkl}}$$

Bragg's law

$$\lambda = 2d_{hkl} \sin \theta$$

P: tie-point

the periodic, complex, dielectric constant :

connection to the Fourier series describing electron densities

o **E & H** small enough -> linear relations

$$4\pi \underline{P} = \chi \underline{E} \quad \underline{D} = \underline{E} + 4\pi \underline{P} = (1 + \chi) \underline{E} = \epsilon \underline{E}$$

$$4\pi \underline{M} = \chi_m \underline{H} \quad \chi_m \neq 0$$

$\chi(\underline{r})$  carries all the physical information about the crystal

$$\chi(\underline{r}) = \sum_{\underline{h}} \chi_{\underline{h}} \exp(-2\pi i \underline{h} \cdot \underline{r})$$

$$\chi_{\underline{h}} = \frac{1}{V} \int \chi(\underline{r}) \exp(2\pi i \underline{h} \cdot \underline{r}) d^3 \underline{r}$$

o sinusoidal field on a collection of free electrons  $m \ddot{\underline{x}} = e \underline{E}$

$$\Rightarrow \underline{x} = -\frac{e}{m\omega^2} \underline{E}$$

$$\underline{P} = e \rho(\underline{r}) \underline{x} = -\frac{e^2}{mc^2} \left(\frac{\lambda}{2\pi}\right)^2 \rho(\underline{r}) \underline{E} \Rightarrow \chi(\underline{r}) = -\frac{e^2}{mc^2} \frac{\lambda^2}{\pi} \rho(\underline{r})$$

o bound electrons  $m \ddot{\underline{x}} = e \underline{E} - m \gamma \dot{\underline{x}} - m \omega_0^2 \underline{x}$

$$\chi(\underline{r}) = -\frac{e^2 \lambda^2}{mc^2 \pi} \rho(\underline{r}) = \text{generalized density}$$

$$\chi_{\underline{h}} = -\Gamma F_{\underline{h}}$$

$$\Gamma = \left(\frac{e^2}{mc^2}\right) \frac{\lambda^2}{\pi V_c}$$

which accounts for the bounded electrons and absorption

$$f \Rightarrow f + f' + i f''$$

$$F_{\underline{h}} = \sum_n \{f_n(s) + f_n' + i f_n''\} e^{-M_n} e^{2\pi i \underline{h} \cdot \underline{r}_n}$$

$$F_{\underline{h}} = F_{\underline{h}}' + i F_{\underline{h}}''$$

refraction index  $n$   $\eta = \frac{c}{v} = \sqrt{\mu' \epsilon} = \sqrt{1 + \chi_0}$   
 average of  $\chi(\epsilon)$

$$\chi_0 = -\Gamma F_0 \quad \text{hkl} = 000$$

$$= -\Gamma F_0' - i\Gamma F_0'' \quad |\chi_0| \approx 10^{-5} - 10^{-6}$$

$$\eta = 1 + \frac{\chi_0}{2} = 1 - \underbrace{\Gamma F_0'}_2 - i \underbrace{\Gamma F_0''}_2$$

reflection      absorption

$$n' = 1$$

$$\text{but } n' < 1$$

$$\Rightarrow |k| < |k|_{\text{vacuum}}$$

total external  
reflection

$$\mu_0 = \left(\frac{2\pi}{\lambda}\right) \Gamma F_0''$$

cut  $k_n$  through G.c.  
 $\mu_0 = 3.80 \text{ cm}^{-1}$   
 $\lambda = 2.54 \times 10^{-8} \text{ cm}$   
 $\Gamma F_0'' = 0.86 \times 10^{-6}$

basic equations for possible wave-fields

Maxwell's equations

$$\nabla \times \underline{E} = -\frac{1}{c} \frac{\partial \underline{H}}{\partial t} \quad \nabla \cdot \underline{H} = 0$$

$$\nabla \times \underline{H} = \frac{1}{c} \frac{\partial \underline{D}}{\partial t} \quad \nabla \cdot \underline{D} = 0$$

$$\Rightarrow \nabla^2 \underline{D} + 4\pi^2 |k|^2 \underline{D} + \nabla \times (\nabla \times \chi \underline{D}) = 0 \quad |k| = \frac{1}{\lambda}$$

$$|\chi|^2 \ll 1$$

$\underline{D}$  sum of plane waves (Bloch's solutions)

$$\underline{D} = e^{2\pi i (\nu t - \underline{k} \cdot \underline{r})} \sum_m \underline{D}_m e^{-2\pi i \underline{h}_m \cdot \underline{r}}$$

or  $\underline{D} = e^{2\pi i \nu t} \sum_m \underline{D}_m e^{-2\pi i \underline{k}_m \cdot \underline{r}}$

with the condition  $\underline{k}_m = \underline{k}_0 + \underline{h}_m$  (Bragg's law)

fundamental equation of the dynamical theory

$$\Rightarrow \frac{k_m^2 - k^2}{k_m} \underline{D}_m = \sum_n \chi_{m-n} \hat{k}_m \times (\hat{k}_m \times \underline{D}_n)$$

$$k = \frac{1}{\lambda} = \frac{\nu}{c}$$

$|\chi_{m-n}|$  very small typically  $\sim 10^{-5}$

-> equation is satisfied for  $D_m$  not vanishingly small only if  $k_m^2 = K^2$   
 i.e. if elastic Bragg diffraction is nearly satisfied.

one-wave case (o)

if only  $D_o$  is non-negligible, i.e. far from the Bragg condition

$$\frac{k_o^2 - k^2}{k_o^2} D_o = \chi_o D_o \Rightarrow k_o^2 (1 - \chi_o) - K^2 = 0 \quad \frac{k_o}{K} = n'$$

$$n' = \frac{1}{\sqrt{1 - \chi_o}} = 1 + \frac{\chi_o}{2}$$

two-wave case (o,h)

Bragg condition nearly satisfied for one set of plans

$$\begin{vmatrix} \frac{k^2 - k_o^2}{K^2} & P \chi_h \\ P \chi_h & \frac{k^2 - k_h^2}{K^2} \end{vmatrix} = 0$$

$$k = K \left(1 + \frac{\chi_o}{2}\right)$$

$$P \equiv \frac{D_o \cdot D_h}{D_o D_h} = \frac{1}{\cos 2\theta_o} \quad \sigma \quad \pi$$

-> spheres of radii  $k$ , centered around O and H

$$(k^2 - k_o^2)(k^2 - k_h^2) = P^2 \chi_h \chi_h K^2$$

$$2K \xi_o \equiv k_o^2 - k^2$$

$$2K \xi_h \equiv k_h^2 - k^2$$

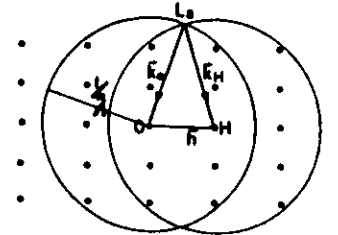
$$\xi_o \xi_h = \frac{P^2 \chi_h \chi_h K^2}{4}$$

$$\frac{D_h}{D_o} = \frac{2\xi_o}{K \chi_h} = \frac{K \chi_h}{2 \xi_h}$$

geometrical approach

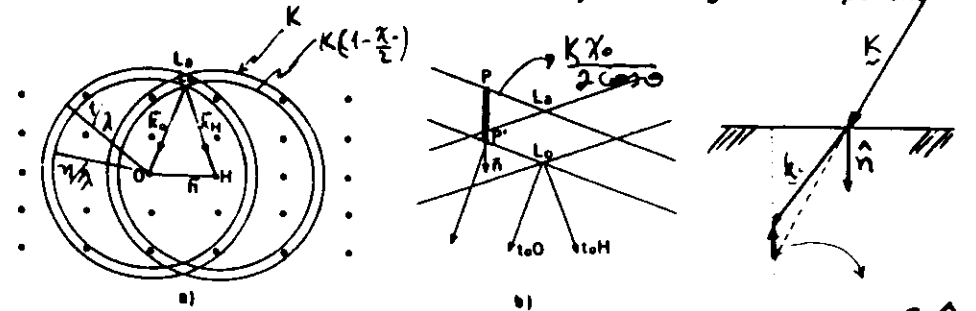
It is interesting to use Ewald's construction to better understand the dynamical parameters.

two spheres of radii  $k$  centered at O and H



refraction ( $n' < 1$ )

to match outside to inside field continuity of the tangential component



$$|K| = \frac{1}{\lambda} = |k_o|$$

$$k_o - k = -K \delta \hat{n}$$

what happens when we are near a Bragg condition?



field equations near a Bragg condition (two-wave case)

$$(k_0^2 - k^2) = (k_0 + k)(k_0 - k) \approx 2K(k_0 - k)$$

$\approx 2K$        $\sim 10^{-5}$

$$\xi_0 \approx k_0 - k$$

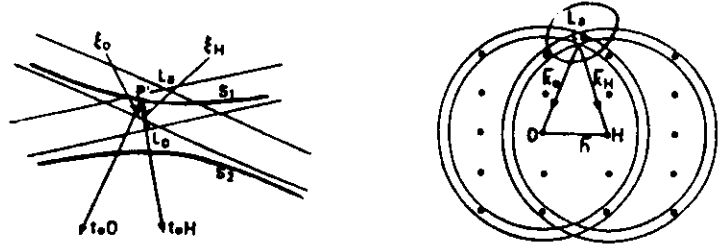
$$\xi_h \approx k_h - k$$

$$\xi_0 \xi_h = \frac{\chi_h \chi_h^* k^2}{4}$$

$$\frac{D_h}{D_0} = \frac{2\xi_0}{K\chi_h} = \frac{K\chi_h}{2\xi_h}$$

the secular equation is transformed into a hyperbola ("two branches")

"dispersion surface"



the dispersion surface contains full information about the waves which can propagate in the crystal

diameter  $S_1 S_2$ :  $\frac{|\chi_h| K}{\cos \theta}$

- the amplitude ratio is proportional to the distance of the tie-points to the asymptotes.
- propagation direction is the normal to the dispersion surface at the corresponding tie-point.

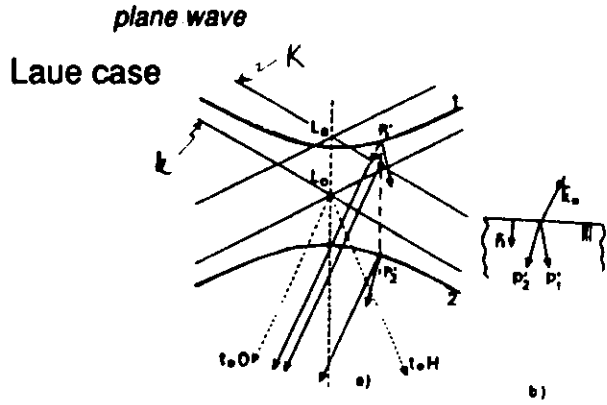
$$\xi_0' \approx k_0' - k$$

$$\xi_0'' \approx -k_0'' \cos \beta - \frac{1}{2} K \Gamma F_0''$$

$\text{for } \left(\frac{k_0''}{k_0'}\right)^2 \ll 1$

boundary conditions at the crystal entrance

the tangential component of the wave-vectors has to be conserved



PO : incoming wave-vector  $k_0$

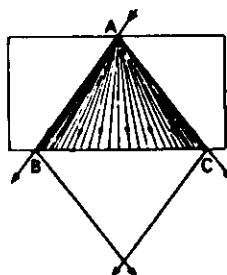
generates two wave-fields inside the crystal  
the propagation direction is normal to the dispersion surface

As  $k_0$  changes by few seconds of arc  
the wave fields change their propagation direction angle  
by the very large angle  $2\theta$

### Borrmann fan

Incident wave :

sufficiently wide spatially to be considered as an almost plane wave, but sufficiently narrow to be traced as bundles of rays.



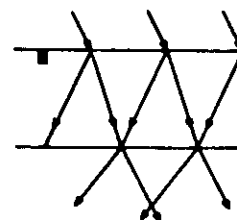
there will be wave-fields propagating in all directions between the incident and the diffracted direction

### Pendellosung effects

the two-wave field excited will overlap through their propagation

O-type fields are coherent ;  $P'_1O$  and  $P'_2O$  differ by  $P'_1P'_2$

the amplitude oscillates along the normal to the entrance surface with a period  $(1/P'_1P'_2)$  as the wave-fields propagate into the crystal.



symmetrical Laue geometry and at exactly the Bragg condition we have the

Pendellosung period :  $\Delta = \frac{1}{S_1 S_2} = \frac{\cos \theta}{k |\chi_h|}$  ( $\Delta \sim 10 \mu m$ )

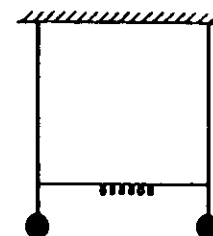
at depth  $\Delta/2$  "O" is zero

•  $0, \Delta, \dots$  "O" is MAXIMUM

H-type fields : initial phase difference  $\pi$  ∴ at  $\Delta/2$ , MAXIMUM  
at  $0, \Delta$ , ZERO

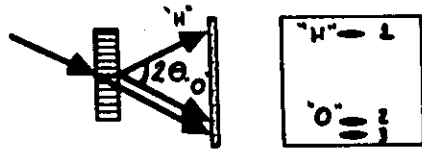
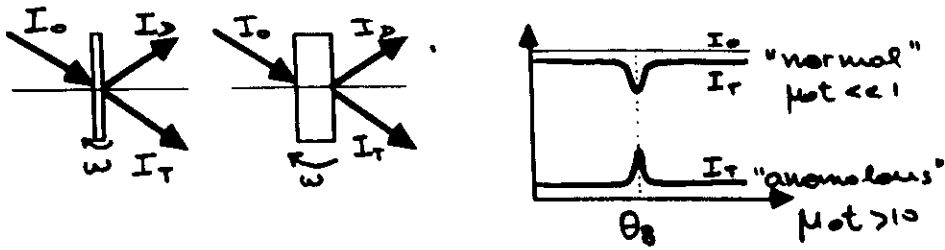
Ewald analogy

coupled pendula



Pendellosung fringes are very sensitive to crystal distortion

**Bormann effect**



some mechanism keeps the energy away from the absorbing atoms

DYNAMICAL THEORY predicts that a STANDING WAVE pattern should exist inside the crystal

tie-point on branch 1 : nodes are on the lattice plans

branch 1 -> branch 2 patterns are shifted by  $\pi$

=> type 1 fields will be less absorbed than type 2 fields

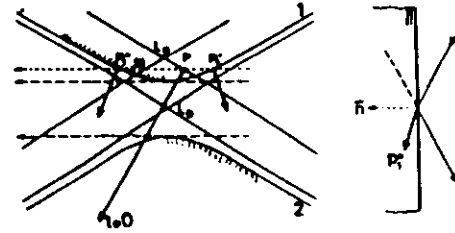
absorbing atoms

Bormann effect :

only branch 1 wave-fields with propagation direction along the plans survive

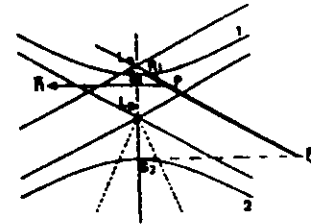
(when nodes becomes points of zero intensity)

**Bragg case**



$P_1$  points out of the crystal and it is not a physical solution (for thick crystals)

**total reflection**

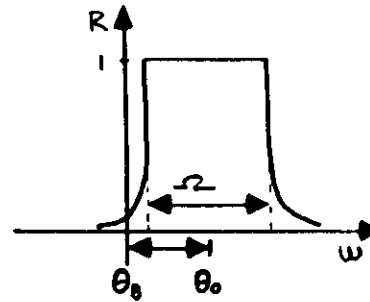


**Darwin width**

$$\Omega = \frac{2|\chi_h|}{\sin 2\theta}$$

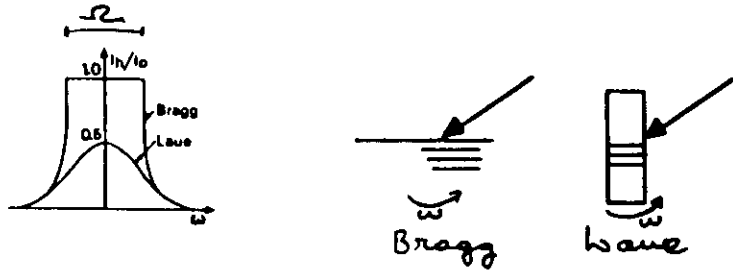
the center is not on the Laue point  
the shift is just the refraction correction

$$\frac{\chi_0}{\sin 2\theta}$$



rocking curves and integrated reflectivity

ideal case

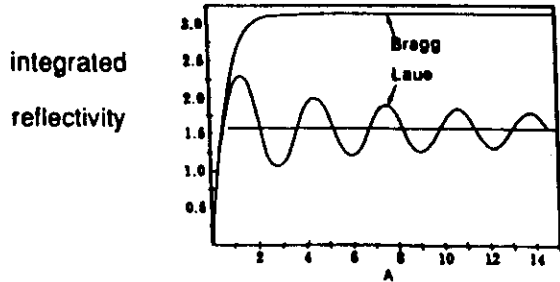


infinitely thick; non-absorbing; symmetrical geometry

Bragg:  $R'_{hkl} = \pi \frac{\Omega}{2} = \frac{\pi \chi_h}{\sin 2\theta}$

$R'_{hkl} = \frac{\pi \chi_h}{\sin 2\theta} \tanh A$       $A = \frac{\pi t}{\Lambda}$       $t$ : thickness  
 $\Lambda$ : Pendellosung period

Laue:  $R'_{hkl} = \{ |\chi_h| / \sin 2\theta \} W(A)$       $W(A) = \int_0^{2A} J_0(u) du$   
 no total reflection      $J_0(u)$  Bessel func.  
 maximum is 0.5



DYNAMICAL THEORY

- the total wave-field inside the crystal is considered as a single entity  
 energy is swapped back and forth between them
- it is necessary whenever diffraction by perfect crystals is involved  
 impose corrections to the kinematical theory (extinction)
- the process is coherent

● interesting effects :

Bragg total reflection

Bormann effect

anomalous transmission  
 polarization

Pendellosung oscillations

very accurate values of structure factors have been obtained

Standing waves

● more general presentation :

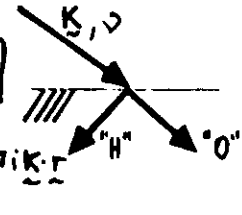
asymmetry

multiple diffraction

extreme situations ( $\theta = 0$  or  $\pi/2$ )

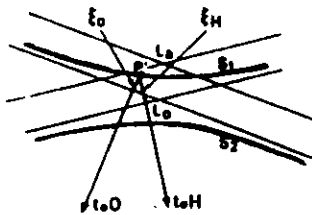
backdiffraction

field equations in the two wave case

$$D = e^{2\pi i \nu t} \left[ D_0 e^{-2\pi i \mathbf{k}_0 \cdot \mathbf{r}} + D_h e^{-2\pi i \mathbf{k}_h \cdot \mathbf{r}} \right]$$


solutions inside the crystal when  $D_{inc} = e^{2\pi i \nu t} D_0 e^{-2\pi i \mathbf{k}_0 \cdot \mathbf{r}}$

dispersion surface



$$\xi_0 \xi_h = \frac{1}{4} k^2 P^2 \chi_h \chi_h \quad 2K \xi_0 \equiv k_0^2 - k^2$$

$$R = \frac{D_h}{D_0} = \frac{2\xi_0}{k \chi_h} = \frac{k \chi_h}{2\xi_h} \quad 2K \xi_h \equiv k_h^2 - k^2$$

$$\mathbf{k}_0 = \mathbf{k} - k \delta \hat{n} \rightarrow \delta = -\frac{\frac{1}{2} k \chi_0 + \xi_0}{k \cdot \hat{n}}$$

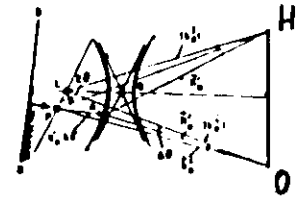
$$|\mathbf{k}| = \frac{1}{\lambda} = |\mathbf{k}_0| = |\mathbf{k}_h| \quad k = k \left(1 + \frac{\chi_0}{2}\right)$$

$\xi$  as a function of  $\theta$

$$\mathbf{k}_h = \mathbf{k}_0 + \mathbf{h}, \quad \xi_0, \xi_h$$

$$a = (2 \mathbf{k}_0 \cdot \mathbf{h} + h^2) / k^2$$

$$b \equiv \frac{\mathbf{k}_0 \cdot \hat{n}}{k_h \cdot \hat{n}} = \frac{\delta_0}{\delta_h}$$



$$\rightarrow \xi_h = \frac{k \chi_0 (1-b)}{2} + \xi_0 \frac{1}{b} + \frac{1}{2} a k$$

using the dispersion relation

$$\xi_0 = \frac{1}{2} k |P| |b|^{1/2} \Gamma [F_h F_h]^{1/2} [\eta \pm (\eta^2 + b/|b|)^{1/2}]$$

$$\xi_h = \frac{1}{2} k |P| (\Gamma/|b|^{1/2}) [F_h F_h]^{1/2} / [\eta \pm (\eta^2 + b/|b|)^{1/2}]$$

where  $\eta \equiv \frac{\chi_0 (1-b) + a \cdot b}{2 |b|^{1/2} (\chi_h \chi_h)^{1/2}}$

• if  $a \approx 2 \Delta \theta \sin 2\theta_B \rightarrow \eta = \frac{b \Delta \theta \sin 2\theta + \frac{1}{2} \Gamma F_0 (1-b)}{\Gamma |P| |b|^{1/2} [F_h F_h]^{1/2}}$

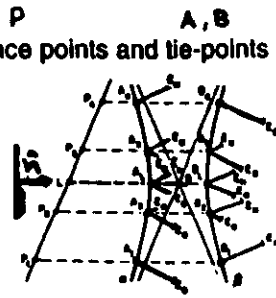
• fundamentally,  $\eta$  is a large constant (complex) times  $\Delta \theta$

$\Delta \theta$  within few seconds of arc  $\leftrightarrow$   $\eta$  within 0 and small integer (pos. or neg)

given  $\frac{\Delta \theta}{\lambda}, b \rightarrow \eta \rightarrow \xi \begin{matrix} \rightarrow \xi' \\ \rightarrow \xi'' \end{matrix} \Rightarrow R, k_0 \text{ and } k_h$

Laue case :  $b/|b| = 1$

relation between entrance points and tie-points



$b=+1$  symmetric

$$S_0 = \frac{1}{2} K |P| |b|^{1/2} \Gamma [F_h F_{\bar{h}}]^{1/2} e^{\pm iV}$$

$$\frac{D_h}{D_0} = \mp \left[ \frac{|P| |b|^{1/2}}{P} \right] \frac{[F_h F_{\bar{h}}]^{1/2}}{F_h} e^{\pm iV}$$

$$\eta = \frac{1}{2} (e^V - e^{-V}) = \sinh V$$

• well off Bragg angle

$$\Delta \theta^2 \sin^2 2\theta \gg P^2 \Gamma F_h F_{\bar{h}}$$

$$S_0' \rightarrow 0 \quad \text{or} \quad \pm K |\Delta \theta| \sin 2\theta \rightarrow A_1 B_4 \quad S_0 \rightarrow 0 \quad \frac{D_h}{D_0} \rightarrow 0$$

$$S_0'' \rightarrow 0$$

NO DIFFRACTED BEAM

and, in addition,

$$k_0' = S_0' + K (1 - \frac{1}{2} \Gamma F_0') \rightarrow K (1 - \frac{1}{2} \Gamma F_0')$$

$$k_0'' \cos \beta = \frac{1}{2} K \Gamma F_0'' - S_0'' \rightarrow \frac{1}{2} K \Gamma F_0''$$

$$\left( e^{-2\pi i k_0 \cdot r} \right)^2 \rightarrow \mu_2 t = 2\pi K \Gamma F_0'' t \quad \mu_2 = \mu_0 = 2\pi K \Gamma F_0''$$

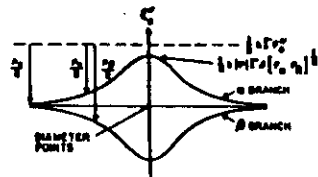
• at Bragg angles (diameter points)

$$\Delta \theta = 0, \quad \eta = 0$$

$$S_0 = S_h = \pm \frac{1}{2} K |P| \Gamma [F_h F_{\bar{h}}]^{1/2}$$

$$S_0'' = \pm \frac{1}{2} K |P| \Gamma \{ [L_m(F_h F_{\bar{h}})]^{1/2} \}$$

$$\frac{D_h}{D_0} = \pm \frac{|P|}{P} \frac{[F_h F_{\bar{h}}]^{1/2}}{F_h}$$



effective absorption

$(e^{-2\pi i k_0 \cdot r})^2$  one of the most interesting aspect of dynamical theory

$$\mu_0(\text{eff}) = \mu_0 \left[ 1 \pm |P| \epsilon (1 - \rho^2)^{1/2} \right]$$

$\mu_0$  normal linear absorption coefficient

$$\rho = \frac{\tan \Delta}{\tan \theta}$$

$\Delta$  the angle between the normal to the dispersion surface and lattice plans

$$P \begin{pmatrix} -1 \\ 0 \\ +1 \end{pmatrix}$$

limits of the dispersion surface

$$\epsilon = \frac{F_0''}{F_0'}$$

(exactly true for centrosymmetric crystals)

$$\mu_0(\text{eff}) = \mu_0 \left\{ 1 \pm |P| \epsilon / [1 + \eta^2] \right\} \quad \eta' = \frac{\Delta \theta \sin 2\theta}{\Gamma |P| F_h'}$$

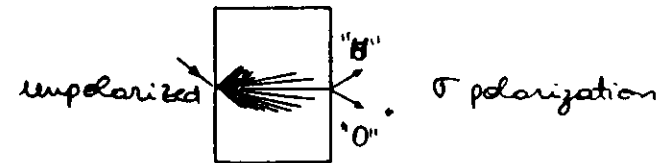
o Borrmann effect

$$\sigma \text{ pol } (P=1); \quad \epsilon = \frac{f''(2\theta)}{f''(0)} = 1$$

$$\Delta = 0 \quad (\rho = 0, \Delta \theta = 0)$$

$$\mu_0(\text{eff}) = \begin{matrix} 0 & \text{or} & 2\mu_0 \\ \text{branch 1} & & \text{branch 2} \end{matrix}$$

$$\text{at } \Delta \theta = 0 \Rightarrow \mu_0(\text{eff}) = \mu_0 [1 \mp |P| \epsilon]$$



# physical interpretation

In terms of the positional dependence of the electric field

- $\eta' = \Delta = \rho = 0$  and  $F_h = F_{h'}$

$$D = e^{2\pi i v t} [D_0 e^{-2\pi i \frac{h_0}{d} \cdot r} + D_h e^{-2\pi i \frac{h}{d} \cdot r}]$$

$$S_0 = S_h \Rightarrow |D_0| = |D_h| \quad \frac{D_h}{D_0} = \pm 1$$

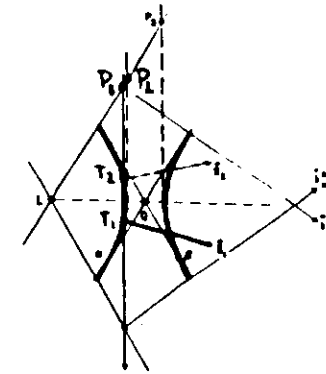
$$\rightarrow |D|^2 = 2 |D_0|^2 (1 \pm P \cos[2\pi \frac{h}{d} \cdot r])$$

phase  $2\pi \frac{h}{d} \cdot r = 2\pi \frac{x}{d}$  plans of equal intensity parallel to  $h$

Borrmann effect	$\sigma$	$P=1$	nodes are ZERO intensity
	$\pi$	$P=\cos 2\theta$	nodes are NOT ZERO intensity

# Bragg case

- Bragg selects two tie points on the same branch but, **only one is excited** (Kohler, Ann.Physik 18, 265(1933))



- region which produces no intersection with the dispersion surface no propagating solutions inside

$$D_0^i = D_0^j \quad ; \quad D_h^e = D_h^j$$

- thick crystal : internal flow is eventually attenuated  $\frac{D_h}{D_0} \rightarrow \left| \frac{D_h^e}{D_0^e} \right|^2$

$$\left( \frac{D_h}{D_0} \right)^2 = \frac{S_0}{S_h} \frac{F_h}{F_{h'}} = |b| [\eta \pm (\eta^2 - 1)^{1/2}]^2 \frac{F_h}{F_{h'}}$$

for  $F_h = F_{h'}$

$$\left| \frac{D_h^e}{D_0^e} \right|^2 = |b| |\eta \pm (\eta^2 - 1)^{1/2}|^2$$

→ Bragg sym ( $b=-1$ ) and with no absorption

$$\eta = (-\Delta\theta \sin 2\theta + \Gamma F_0) / |P| \Gamma F_h \quad F_0, F_h \text{ real}$$

$$\eta = +1 \quad \Delta\theta = \frac{\Gamma F_0 - |P| \Gamma F_h}{\sin 2\theta}$$

$$\eta = -1 \quad \Delta\theta = \frac{\Gamma F_0 + |P| \Gamma F_h}{\sin 2\theta}$$

$$\frac{|D_h|^2}{|D_0|^2} = 1$$

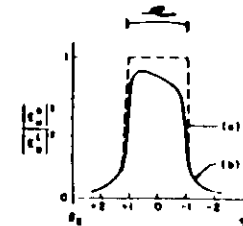
$$\rightarrow \Delta = \frac{2 |P| \Gamma F_h}{\sin 2\theta}$$

solutions surfaces

→ with absorption

$$\eta' = (-\Delta\theta \sin 2\theta + \Gamma F_0') / |P| \Gamma F_h'$$

$$\eta'' = -(F_h'' / F_h') (\eta' - 1 / |P| \epsilon)$$



# primary extinction

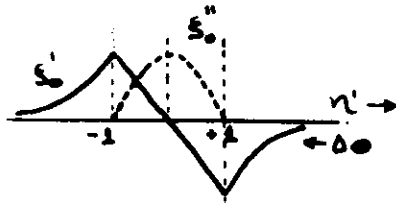
Bragg case with no absorption and  $F_h = F_{\bar{h}}$

$$S_0 = \frac{1}{2} K |P| \Gamma F_h [\eta \pm (\eta^2 - 1)^{1/2}]$$

within the region

$$|\eta| < 1 \quad S_0' = \frac{1}{2} K |P| \Gamma F_h \cdot \eta$$

$$S_0'' = \frac{1}{2} K |P| \Gamma F_h (1 - \eta^2)^{1/2}$$



with  $F_0'' = 0 \rightarrow S_0'' = -k_0'' \sin \theta$

$$\rightarrow e^{-4\pi k_0'' z} = e^{[-2\pi K |P| \Gamma F_h (1 - \eta^2)^{1/2} / \sin \theta] z}$$

$z$  depth in the crystal

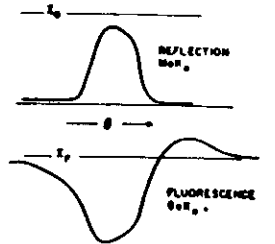
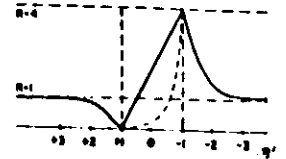
average value of the EXTINCTION FACTOR

$$\exp\left[-\frac{1}{2} \pi^2 K |P| \Gamma F_h / \sin \theta\right] z$$

\* many times greater than normal absorption

# standing waves

wave fields inside the crystal



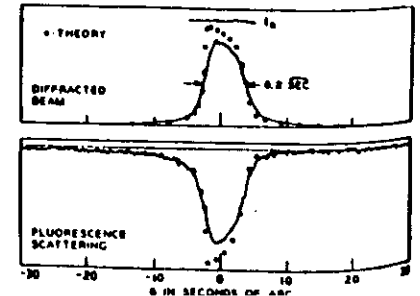
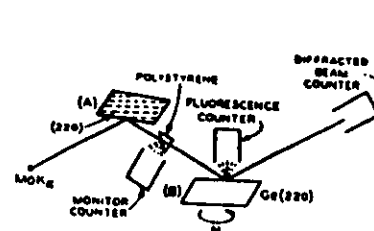
PHYSICAL REVIEW

VOLUME 133, NUMBER 2A

2 FEBRUARY 1964

## Effect of Dynamical Diffraction in X-Ray Fluorescence Scattering

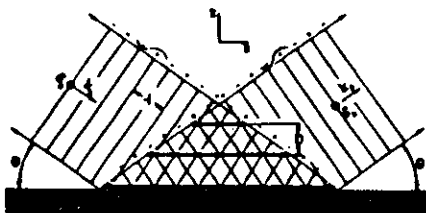
IRVING W. BATTERMAN  
Bell Telephone Laboratories, Murray Hill, New Jersey  
(Received 21 August 1963)



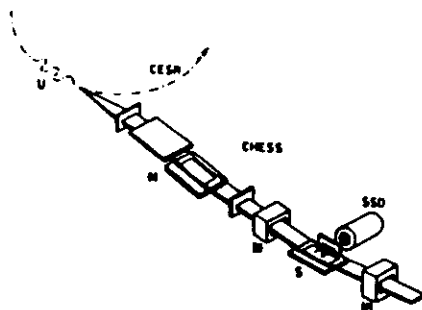


# standing wave technique

- o generation of a standing wave field by the interference of the incident and reflected beams.



- o structural information is obtained by measuring the fluorescence yield from foreign atoms, which depends on the position of such atoms relative to the crystal's diffraction planes



## Observation of internal x-ray wave fields during Bragg diffraction with an application to impurity lattice location\*

Jene A. Golovchenko<sup>1</sup>

<sup>1</sup>Bell Laboratories, Murray Hill, New Jersey 07974  
and Brookhaven National Laboratory, Upton, New York 11973

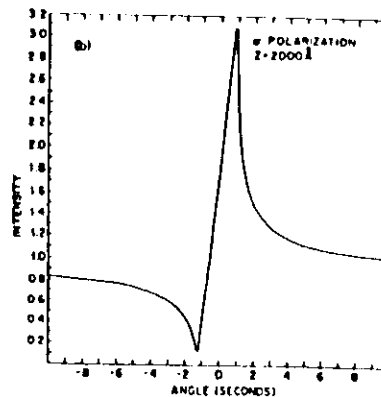
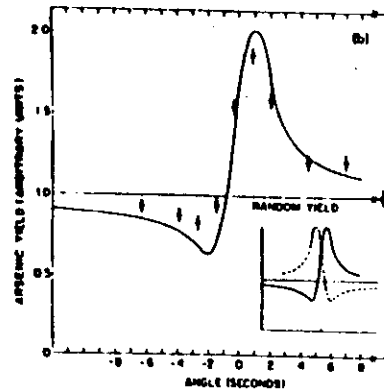
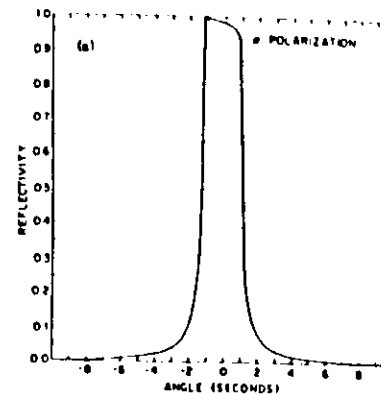
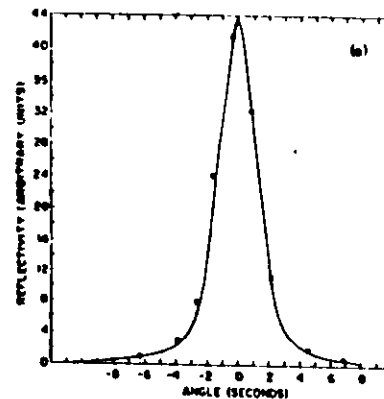
Boris W. Batterman

Cornell University, Ithaca, New York 14850

Walter L. Brown

<sup>2</sup>Bell Laboratories, Murray Hill, New Jersey 07974

(Received 25 June 1974)



**X-Ray Standing Waves at Crystal Surfaces**

P. L. Cowan,<sup>(\*)</sup> J. A. Golovchenko, and M. F. Hobblin  
 Bell Laboratories, Murray Hill, New Jersey 07974  
 (Received 17 March 1980)

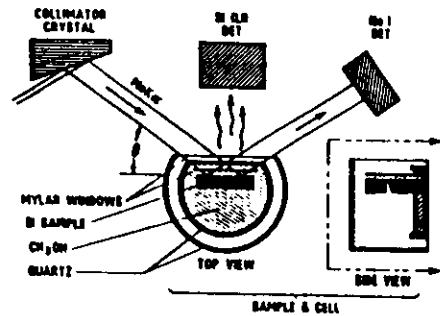
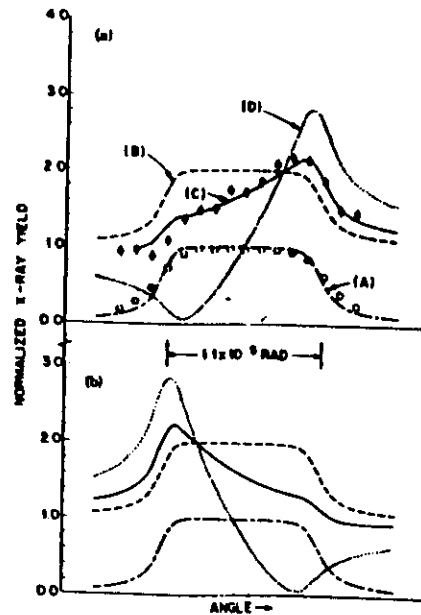


FIG. 1. Schematic layout of experimental apparatus including sample cell detail.



**Simple X-Ray Standing-Wave Technique and Its Application to the Investigation of the Cu(111)( $\sqrt{3} \times \sqrt{3}$ )R30°-Cl Structure**

D. P. Woodruff, D. L. Seymour, C. J. McConville, C. E. Riley, M. D. Crapper, and N. P. Prince  
 Physics Department, University of Warwick, Coventry CV47AL, England

and

Robert G. Jones

Chemistry Department, University of Nottingham, Nottingham NG72RD, England  
 (Received 10 October 1976)

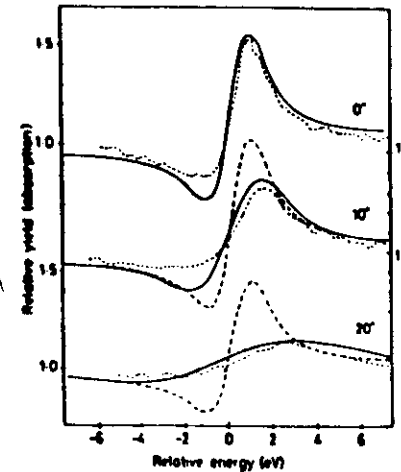


FIG. 1. Relative Cu 2p-derived Auger-electron yield (short dashed lines) from Cu(111) as the photon energy is scanned through the (111) Bragg reflection for incidence angles of 0° (normal incidence), 10°, and 20° compared with theoretical absorption profiles at the atomic planes incorporating random angular standard deviations of 0.01° (long dashed lines) and 0.1° (solid lines). For 0° incidence the two theoretical lines are indistinguishable.

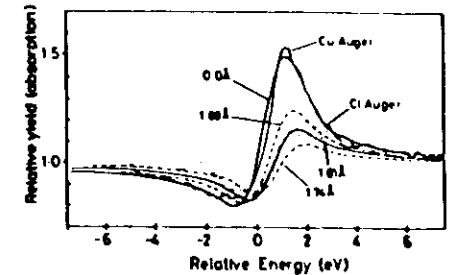


FIG. 2. Relative Cu 2p-derived and Cl 1s-derived Auger-electron yields from Cu(111)( $\sqrt{3} \times \sqrt{3}$ )R30°-Cl as the photon energy is scanned through the (111)  $\sqrt{3} \times \sqrt{3}$  reflection at normal incidence. Also shown are theoretical absorption curves for absorption on the Cu atom planes and at 1.7, 1.8, and 1.88 Å above the last Cu atom plane of a perfect substrate. In these theoretical curves only 80% of the Cu or Cl absorbers are assumed to be coherently positioned relative to the substrate lattice.

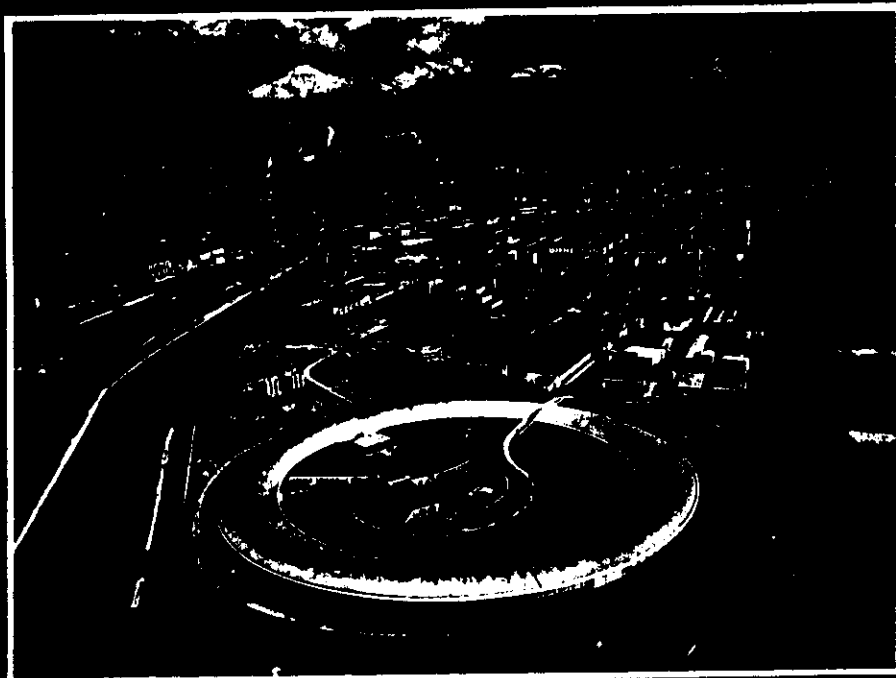
Additional material to the lecture

“Dynamical Theory of X-ray Diffraction  
by Perfect Crystals”

by Hélio Tolentino



# NEUTRON AND SYNCHROTRON RADIATION FOR CONDENSED MATTER STUDIES



HERCULES

M. SCHLENKER

Both in the HERCULES course and in this volume, this should be the transition from scattering by single atoms (Chap. I) to scattering by assemblies of many atoms. We will focus on elastic scattering by crystals. Actually, many of the results we will derive here were already encountered in Chap. III and V in the description of optical devices for synchrotron radiation and neutron beam conditioning based on total reflection, and especially on Bragg diffraction by crystals.

This Chapter contains three parts. Section VI.1 is devoted to standard aspects of diffraction. We will introduce the reciprocal lattice, a concept central to diffraction physics as well as to solid state physics at large. The reflectivities will be discussed in the kinematical approximation, for which, to begin with, we use a restrictive definition, that of very thin crystals where the diffracted amplitude is negligible compared to the incident amplitude. These results are elementary, largely familiar to whoever had an exposure to crystallography, and very heavily used in structural crystallography. We will also note that much of the fundamentals, e.g. the simple, Fourier-transform, relationship between the diffracted intensity distribution and the pair-correlation function, is common to all parts of elastic scattering, and also used in diffuse scattering and small angle scattering.

Section VI.2 covers the dynamical treatment of diffraction by perfect, large crystals. It should be clear to every user of synchrotron radiation that perfect, large crystals actually exist, and that, as shown in Chap. III, most optical elements are based on diffraction by such perfect silicon crystals, and must be described by dynamical theory. It is therefore not just an academic curiosity.

Section VI.3 will return to the kinematical limit. We will see that kinematical behavior is also encountered in crystals that are not very small, provided they are very imperfect. This section will also briefly outline the difficult description of diffraction by crystals of intermediate (im)perfection, i.e. extinction.

Chap. VII and VIII will be devoted to the actual methods of diffraction work for structural investigations, i.e. the determination of the average microscopic structure, Chap. IX to the overall investigation of defects (diffuse scattering) and Chap. X to the study of large-scale inhomogeneities (small-angle scattering). Chap. XVII will show how the features of dynamical diffraction by perfect or almost perfect crystals can be used to image individual defects and domains.

## VI.1. General features of neutron and X-ray diffraction in the kinematical approximation

### VI.1.1. Diffracted amplitude in the kinematical approximation.

Consider a plane, monochromatic wave, with amplitude  $\psi_1$  and wave-vector  $k_0$ , impinging on a small specimen. The simplifying assumption leading to the kinematical approximation is that the magnitude of the incident wave amplitude is the same at all points in the specimen, with only the phase changing from point to point. This implies that the scattered amplitude be small enough that, at the cost of disregarding the conservation of energy, we can neglect it. It also involves neglecting absorption.

But then the treatment made in Chap. I for a "single" object (Born approximation) can be used: there will be, at large distances from the specimen, a scattered wave expressed, in the *neutron* case, by

$$\psi_{\text{scatt}}(r) = -\psi_1 \frac{2\pi m}{\hbar^2} \frac{e^{2\pi i k r}}{r} \cdot \tilde{V}(K) \quad (\text{equ. I.104 in Chap. I})$$

This is a spherical wave (nearly a plane wave since  $r$  is large), with amplitude proportional to the Fourier transform of the potential over the region of interest.

In this chapter, unlike in Chap. I, the Fourier transform is distinguished by the tilda as well as by the fact that the variable is a reciprocal length.  $K = k - k_0$ , where  $k$  is a vector along  $r$ , the vector from the origin  $O$ , chosen inside the specimen, to observation point  $P$  and its magnitude is here defined in the crystallographers' convention, viz.  $k = 1/\lambda$ , with  $\lambda$  the wavelength in vacuum.

The potential (actually the potential energy) is the Fermi pseudo-potential.

Similarly, for *X-rays*, the diffracted amplitude is proportional to the Fourier transform  $\tilde{\rho}(K)$  of the electron density  $\rho(r)$ . The fact that only electrons are effective is simply due to the fact that, in comparison with the other charges present in materials, viz. nuclei, they are lighter, and therefore have accelerations at least  $2.10^3$  times bigger than the nuclei. However X-rays are electromagnetic waves and thus vectorial, not scalar. Since the scattered electric field must be perpendicular to the wave-vector, only the projection of the incident wave's electric field along the normal to the scattered direction is effective in producing scattering. This was briefly discussed at the end of I.3.1. It can be handled easily by introducing, in the expression for the scattered amplitude, a polarization coefficient  $C_1$  multiplying  $\tilde{\rho}(K)$ . For the two principal polarization states of the incident beam,  $\sigma$  ( $E$  perpendicular to the scattering plane, defined as the plane containing  $k_0$  and  $k$ ) and  $\pi$  ( $E$  in the scattering plane), it takes the values  $C_\sigma = 1$  and  $C_\pi = \cos 2\theta$ , where  $2\theta$  is, in this Chapter, the scattering angle.

### VI.1.2. Geometry: the reciprocal lattice

Every microscopic quantity in a crystal has spatial periodicity, and can be described by the convolution of a "pattern" function defined within one period by the Poisson distribution, a periodic repetition of Dirac distributions.

In the one-dimensional case

$f_{\text{periodic}}(x) = f_{\text{one period}}(x) * P_{[a]}(x)$  if  $a$  is the period, with

$$P_{[a]}(x) = \sum_{\text{all } n} \delta(x-na) \text{ the Poisson distribution.}$$

Since the Fourier transform of  $P_{[a]}(x)$  is also a Poisson distribution, with period  $1/a = a^*$ , we can write

$$\text{FT} \{P_{[a]}(x)\} = \tilde{P}_{[a^*]}(k) = \text{const.} \cdot \sum_{\text{all } h} \delta(k-h.a^*) \text{ with } h \text{ an integer.}$$

The Fourier transform in this one-dimensional case is non-zero only when the wave-number is a multiple of  $a^*$ . This is a familiar result: any periodic function can be expanded into a Fourier series, instead of a Fourier integral.

So the Fourier transform of  $f_{\text{periodic}}$  is a set of Dirac distributions, with the amplitude of each determined by the Fourier transform of the pattern  $f_{\text{one period}}$ :  $\text{FT}\{f_{\text{periodic}}(x)\} = \tilde{f}(k) = \text{FT}\{f_{\text{one period}}(x)\} \cdot \tilde{P}_{[a^*]}(k)$  (fig. VI.1).

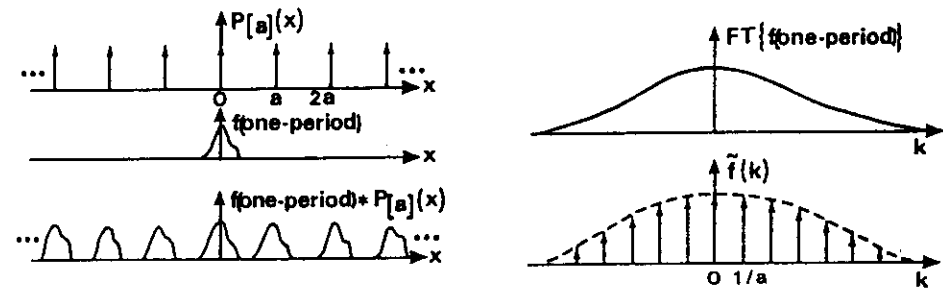


Fig. VI.1. -- A periodic function of one variable (a one-dimensional model of a crystal) as the convolution of a Poisson distribution  $P_{[a]}(x)$  by the function over one period,  $f_{\text{one period}}(x)$ . Its Fourier transform (FT) is the product of the FT of  $f_{\text{one period}}(x)$  by the FT  $\tilde{P}_{[a^*]}(k)$  of the Poisson distribution, and is therefore non-zero only for  $k=p.a^*=p/a$ , with  $p$  an integer.

On carrying this over to three dimensions, the period is replaced by three vectors, the basis vectors  $a, b, c$  of the lattice. We have to build a three-dimensional Fourier series, breaking up  $V(r)$  into a series of plane waves,

$$V(r) = \sum_{\text{all } K} V_K e^{i2\pi K \cdot r} \text{ with wave-vectors } K \text{ which have to ensure that}$$

$$V(r + ua + vb + wc) = V(r), \text{ hence that } K \cdot r = K \cdot (r + ua + vb + wc) \text{ if } u, v, w \text{ are}$$

This is satisfied if  $K = ha^* + kb^* + lc^*$  where  $a^*, b^*, c^*$ , the basis vectors of the reciprocal lattice, satisfy the two conditions:

$$a^* \cdot a = b^* \cdot b = \dots = 1 \text{ and } a^* \cdot b = a^* \cdot c = \dots = 0.$$

It is easy to check that these conditions are satisfied with

$$a^* = (b \times c) / V_c; b^* = (c \times a) / V_c \text{ etc., where } x \text{ means the cross product, and } V_c = a \cdot (b \times c) \text{ is the volume of the unit cell.}$$

Two useful properties of reciprocal lattice vectors  $h = ha^* + kb^* + lc^*$  (with  $h, k, l$  integers) are that  $h$  is perpendicular to the lattice planes with Miller indices  $(hkl)$  of direct space, and that its modulus  $|h|$  is the reciprocal of the distance between successive  $(hkl)$  lattice planes:  $|h| = 1/d_{hkl}$ .

One of the conditions for non-zero scattered intensity from a periodic distribution of potential in space, with the periodicity characterized by the direct-space lattice, is therefore that  $K = k - k_0$  equal a reciprocal-lattice vector  $h$ .

Another way of getting the same result is to note that, whenever a given array of scatterers is repeated periodically (on a lattice), the contributions to diffraction with a change in wave-vector  $K$  will only add (interfere constructively) if  $K \cdot a = h$  with  $h$  integer etc. This condition (Laue's condition) can also be retrieved easily by drawing wave-fronts, and calculating the phase shifts between the contribution of different scattering arrays.

Thus the positions of the nodes of the reciprocal lattice give the periodicity of  $V(r)$ , or  $\rho(r)$ , hence of the crystal. But they do not tell what the unit cell contains.

Bragg scattering is coherent elastic scattering by a crystal. The word "elastic" contains another condition: there can be no change in the magnitude of the wave-vector in vacuum, hence  $k = 1/\lambda = k_0$ .

As a result, the condition for Bragg scattering from a crystal can be fully expressed geometrically in Ewald's construction. Draw the reciprocal lattice. Pick one node as the origin of reciprocal space,  $O$ . Mark the wave-vector of the incident wave, in direction and magnitude, with its end at  $O$ , and call its origin  $P$ . Draw a sphere with center  $P$ , radius  $k = 1/\lambda$ . Of course this sphere, called Ewald's sphere, goes through  $O$  the origin. The diffracted beam's wave-vector (we approximate the diffracted wave by a plane wave), drawn with its origin at  $P$ , must have its end on the sphere to ensure  $k = k_0$ , and it must satisfy  $k = k_0 + h$ . This means that its end must be on a node of the reciprocal lattice (fig. VI.2a).

Thus there will be a diffracted beam if and only if Ewald's sphere goes through the origin and another reciprocal-lattice node. In this case one says that reflection  $h$  is excited, usually spelling out the indices  $hkl$  explicitly, or that the incident beam is Bragg-reflected (or Bragg-diffracted) by the lattice planes  $(hkl)$ .

Bragg's law follows immediately from the above construction:  $2k \sin \theta = |h|$ , so that, since  $|h| = 1/d_{hkl}$ , we get  $2d_{hkl} \sin \theta = \lambda$ .

Note that we write  $2\theta$  for the scattering angle. The angle  $\theta$  satisfying the Bragg-diffraction condition is often noted  $\theta_B$ , and is called the Bragg angle.

The reason for using the word "reflection" is clear from the direct-space situation (fig. VI.2b): since  $h$  is perpendicular to the planes  $(hkl)$  of the (direct) lattice, the incident and diffracted beams have equal glancing angles (angles with

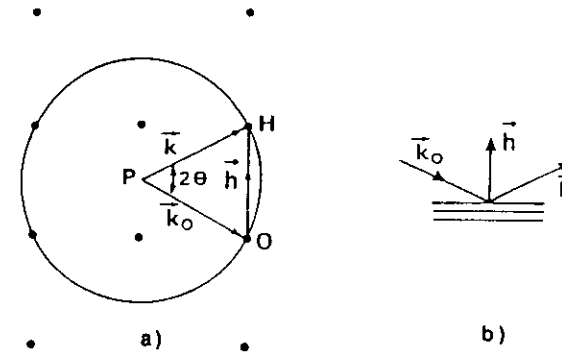


Fig. VI.2 a. — Ewald's construction, in reciprocal space, as the condition for diffraction  $h$  to be excited. The incident wave-vector is  $k_0$ , the diffracted wave has wave-vector  $k$  at large distance from the specimen, with  $k=k_0$  (elastic scattering) and  $k=k_0+h$ . Note that this figure actually corresponds to simultaneous excitation of more than one diffraction.

Fig. VI.2 b. — The Bragg reflection or diffraction process seen in direct space.

the planes)  $\theta$  with the "reflecting" planes. This is reminiscent of the behavior of light on a surface. The difference is that, in diffraction by a periodic structure, reflection only occurs for special wavelengths at given angle, or at special angles for a given wavelength. Physically, one more picture may be useful. The crystal can be considered as the superposition of many plane-wave (Fourier) components of whatever microscopic quantity is of interest. Measuring Bragg diffraction  $h$  means sensing the Fourier component with wave-vector  $h$ .

Naturally, if more than one node other than the origin lies on the Ewald sphere, more than one diffracted beam is produced. This is multiple, or simultaneous, diffraction.

The fact that the crystal is finite implies that the Fourier transform of the potential should not be represented by Dirac peaks (infinitely sharp geometrical points). Describing the direct space potential involves multiplication by a box function, hence the reciprocal space distribution will involve convolution by the Fourier transform of the box function, i.e. a sinc function (defined as  $\text{sinc}(u) = \frac{\sin u}{u}$ ) in one dimension (fig. VI.3). A reciprocal-space volume, corresponding to a three-dimensional sinc function, will thus appear at each node position instead of the unphysical point. It is broad if the crystal is small.

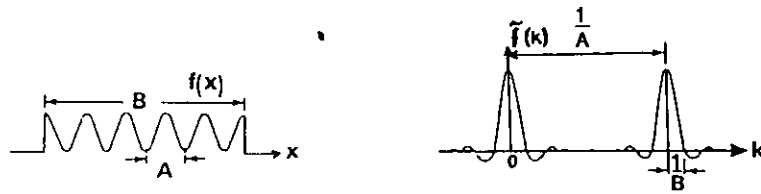


Fig. VI.3. -- A finite crystal in one dimension as a periodic function truncated through multiplication by a box function, and its Fourier transform, with sinc functions replacing the Dirac distributions.

VI.1.3. Weight of reciprocal lattice nodes: the structure factor

Consider first the neutron case, with nuclear scattering only, and no nuclear spin.

It is convenient to consider that the weight of each node, say  $h$ , is just the Fourier coefficient of  $V$  corresponding to this wave-vector, i.e. the amplitude  $V_h$  of the plane-wave component with wave-vector  $h$  of the Fermi pseudo-potential.

It is customary to write the Fourier series decomposition as

$$V(r) = \sum_{\text{all } h} V_h e^{i2\pi h \cdot r}$$

in which case  $V_h = \frac{1}{V_c} \int_{\text{unit cell}} V(r) e^{-i2\pi h \cdot r} d^3r$ . But the pseudo-potential in the unit cell, containing nuclei  $i$ , with scattering length  $b_i$ , at rest at positions  $r_i$ , is

$V(r) = \frac{2\pi\hbar^2}{m} \sum_{i \text{ in unit cell}} b_i \delta(r-r_i)$ , by a straightforward extension of equ. I.98 of Chap. I, and therefore

$$V_h = \frac{2\pi\hbar^2}{mV_c} \int_{\text{unit cell}} \sum_i b_i \delta(r-r_i) e^{-i2\pi h \cdot r} d^3r = \frac{2\pi\hbar^2}{mV_c} \sum_{\text{unit cell}} b_i e^{-2\pi i h \cdot r_i}$$

Another way of writing this is  $V_h = (2\pi\hbar^2/mV_c) \cdot F_h$ , defining the structure factor corresponding to node  $h$  of the reciprocal lattice (or, we will shortly see why, to Bragg reflection  $h$ ) as  $F_h = \sum_{\text{unit cell}} b_i e^{-2\pi i h \cdot r_i}$  [neutrons].

Note that the structure factor, in the neutron diffractionists' usage, is a length.

X-rays are sensitive, via Thomson scattering, to electron density. The

Chap. I (equ. I.53) as for the neutron case, by a scattering amplitude  $-r_0 \tilde{\rho}(K)$ , with  $\tilde{\rho}(K)$  the Fourier transform of the electron density in the crystal.  $r_0 = 2.8 \cdot 10^{-15}$  m is the classical electron radius.

Since the electron density  $\rho(r)$  is periodic too, the relevant quantity is the Fourier component  $\rho_h$ , and it is customary to write a structure factor  $F_h = \rho_h \cdot V_c$ .

The standard expression, which would be valid if the atoms were at rest, is

$F_h = \sum_{\text{unit cell}} f_{at,i}(h) \cdot e^{-2\pi i h \cdot r_i}$  [X-rays], where  $f_{at,i}(h)$  is the atomic scattering factor or form factor for atom  $i$ , at position  $r_i$ . As discussed in Chap. I, this is usually

taken as  $f_{at,i}(h)$ , and tabulated as a function of  $\frac{\sin\theta}{\lambda}$ , i.e.  $\frac{1}{2d_{hkl}}$ .

In the X-ray diffractionists' usage the structure factor is a number, the ratio of the amplitude diffracted by one unit cell to that diffracted by one free electron placed at the origin. Comparison between neutron and X-ray situations is easy to perform by transcribing  $F^n$  (for neutrons) into  $r_0 \cdot F^X$  (for X-rays).

A node with zero associated weight (zero structure factor) is said to be absent, or not to exist. It does not give rise to diffraction. Systematic absences of nodes, hence of reflections, can be related to the choice of a non-primitive unit cell, or to the presence of non-symmorphic symmetry elements. They are most valuable in determining the space group, an essential part of the structural information.

Even in an idealized description, we must take into account the fact that atoms are not at rest, and have a displacement from the average position  $r_i$ . Let  $\rho(r-r_i)$  represent the electron density in an atom at rest, with its center at position  $r_i$ , and let  $p(r_i)$  be the probability density that the center of the atom is at  $r_i$ . Then the electron density of the displaced atom will, on the average, be

$\rho_{av}(r) = \int \rho(r-r_i) \cdot p(r_i) dr_i$ . This is the convolution,  $\rho(r) * p(r)$ , of the electron density by the probability density describing the displacement. In the Fourier transform, this will lead to multiplying the scattering length or atomic scattering factor of each atom  $i$  by a factor  $e^{-W_i}$  (the temperature factor, or the square root of the Debye-Waller factor).  $W_i$  involves the mean square displacement  $\langle u^2 \rangle$  of the atom around its equilibrium position. In the harmonic, isotropic approximation,  $W_i = 8\pi^2 \frac{\sin^2\theta}{\lambda^2} \cdot \langle u^2 \rangle$ . This leads to a significant decrease in scattered intensity

when the sample temperature is high, for light atoms, and for high-order reflections (small  $d_{hkl}$ ). The final expressions for the structure factors are

$$F_h = \sum_{\text{unit cell}} b_i \cdot e^{-2\pi i h \cdot r_i} \cdot e^{-W_i} \text{ [neutrons] and}$$

$$F_h = \sum_{\text{unit cell}} f_{at,i}(h) \cdot e^{-2\pi i h \cdot r_i} \cdot e^{-W_i} \text{ [X-rays]}$$



Thus the information about the distribution of potential, or of atoms, within the unit cell is contained in the structure factors associated with the various nodes of the reciprocal lattice.

#### VI.1.4. Integrated reflectivities

Standard structural crystallography never involves the use of plane waves. The incident beam is always slightly divergent and includes a finite range of wavelengths. Thus the situation we discussed was over-simplified, and we must include the effect of rotating the incident beam, or adding components with a range of directions of the wave-vectors, or, equivalently, rotating the crystal.

The nodes of the reciprocal lattice will then move through reciprocal space, and some of them will go through the Ewald sphere. We have seen that they are little volumes instead of geometrical points, hence there will be diffracted amplitude over a range of crystal rotation, broad if the crystal is very small. The curve of diffracted intensity vs crystal rotation angle  $\omega$  is called the rocking curve.

The information that is of value when the beam is not parallel is the area under the rocking-curve. However this will be in any case proportional to the incident beam intensity  $I_0$  and to the measuring time at each point of the curve, or the reciprocal of the scanning angular velocity. The relevant quantity is therefore the total number of counts  $N_{hkl}$  for the reflection, scaled by  $I_0/\omega'$  where  $\omega'$  is the angular velocity. This is called the integrated reflectivity  $R_{hkl}$  or  $R_h$ .

As derived e.g. in Schwartz & Cohen (1987), the simplest case, corresponding directly to the above discussion (rotating crystal), yields the following expression after integration over the reciprocal-space volume around a node: with  $v$  the volume of the crystal,  $\theta$  the Bragg angle,

$$R_{hkl} = \lambda^3 \frac{|F_h|^2}{V_c^2} \frac{1}{\sin 2\theta} v \text{ for the neutron case } (F_h \text{ is a length})$$

$$R_{hkl} = \lambda^3 \cdot r_0^2 \cdot \frac{|F_h|^2}{V_c^2} \frac{1 + \cos^2 2\theta}{2} \frac{1}{\sin 2\theta} \cdot v \text{ for the X-ray case } (F_h \text{ is a number});$$

The  $1/(\sin 2\theta)$  term, called the Lorentz factor  $L$ , is related to the time the reciprocal lattice volume around a node takes to go through the Ewald sphere during the scan, hence it depends only on the geometry used. Expressions for  $L$  corresponding to all usual single-crystal diffraction methods are given e.g. in International Tables for Crystallography.

The factor  $(1 + \cos^2 2\theta)/2$  in the X-ray expression is called the polarization factor  $P$ . The form written here assumes that the incident beam is unpolarized. Then half of the incident intensity corresponds to  $\sigma$ -polarization, for which  $C_\sigma = 1$ , and half to  $\pi$ -polarization, with the polarization coefficient for the amplitude  $C_\pi = \cos 2\theta$ . The two intensities add because they are incoherent. Other forms apply to synchrotron radiation, which is naturally polarized, or to setups involving a monochromator.

The product (LP) is often termed the "Lorentz-polarization" factor. For a

$$R_{hkl} = \text{constant} \cdot (\text{LP}) \cdot |F_{hkl}|^2$$

with LP easily obtained from the experimental setting. Integrated reflectivities give the relative values of the moduli squared of the structure factors.

#### VI.1.5. The pair-correlation function, the Patterson function, and Friedel's law.

If X-ray or neutron detectors could measure complex amplitudes, including the phase, crystallography would not be a part of science. It would be possible to obtain full crystal structures just by Fourier transforming the distribution of scattered amplitudes. The fact that only intensities are measured, and that the phase of each reflection is not available from measurement, means that a simple Fourier transformation of the experimental data does not directly yield the electron density.

It does, however, provide something useful. The Fourier transform of the product of two functions is the convolution of their Fourier transforms. In the X-ray case, with anomalous scattering neglected, the scattered intensity  $I_{\text{scatt}}$  is proportional to  $\tilde{\rho}(\mathbf{K}) \cdot \tilde{\rho}^*(\mathbf{K}) = \tilde{\rho}(\mathbf{K}) \cdot \tilde{\rho}(-\mathbf{K})$ . Hence by Fourier-transforming the scattered intensity, expressed as a function of wave-vector  $\mathbf{K}$ , we obtain a function of  $\mathbf{r}$ :

$$\rho(\mathbf{r}) * \rho(-\mathbf{r}) = \int_{\text{all space}} \rho(\mathbf{u}) \cdot \rho(\mathbf{u} + \mathbf{r}) d^3\mathbf{u}, \text{ i.e., to within a factor involving the volume,}$$

the density-density correlation function or pair-correlation function, or Patterson function,  $P(\mathbf{r})$ . This function only takes on non-zero values if there is appreciable density both at  $\mathbf{u}$  and at  $\mathbf{u} + \mathbf{r}$ , i.e. at points separated by  $\mathbf{r}$ .

This basic result is used again and again, not only in diffraction by crystals, but also in small-angle scattering and in diffuse scattering.

We note that, under the assumption of no anomalous scattering,  $\tilde{\rho}(-\mathbf{K}) = \tilde{\rho}^*(\mathbf{K})$  and  $I_{\text{scatt}}(\mathbf{K}) = I_{\text{scatt}}(-\mathbf{K})$ . This is known as Friedel's law. It means that, neglecting anomalous scattering, the diffraction pattern shows centrosymmetry whether the crystal is centrosymmetric or not. The symmetry of the diffraction pattern is therefore described by the Laue class (the point group with centrosymmetry added if it is not there).

The phase problem has been fought vigorously, and quite successfully, for many years. A good review on the "direct" methods is given by Hauptman (1991). The use of simultaneous, or multiple, reflections makes it possible to measure the relative phases of different reflections. This will be briefly discussed in VI.2.

#### VI.1.6. X-ray and/or vs neutron diffraction?

Neutron and X-ray scattering are both similar and, through their differences, complementary. One of the keys to designing good experiments is understanding these aspects. It may be a good investment to spend some time browsing through tables of values in the International Tables for Crystallography

Since wavelengths are similar for X-rays and neutrons, so are the Bragg angles, hence the scattering geometry and the formal description. The orders of magnitude of the scattering lengths for atoms are the same, with slightly smaller values for neutrons, at least for small scattering vectors (low index reflections).

Absorption was dismissed in a cursory way in VI.1.1. Except when the Borrmann effect sets in (very perfect crystals, see VI.2.2.6), its treatment is easy in principle: the intensity is affected by a factor  $e^{-\mu t}$  where  $\mu$  is the linear absorption coefficient and  $t$  the path length. In crystals with a complicated shape, however, this is not straightforward even for a computer. In most cases, absorption of neutrons is very small, but absorption of X-rays is not. Lead is an extreme example: it is heavily absorbing for X-rays (hence its use in shielding), but practically not at all for neutrons. Only a few elements, or more exactly isotopes, have strong absorption cross-sections for neutrons: e.g. lithium, boron, cadmium, gadolinium, uranium. There is obviously no direct relation with atomic weight, whereas the relation is simple in the X-ray case.

The neutron cross-sections for nuclear scattering are associated with the strong force. They are not directly related with the atomic number as is the case for X-rays. Structural work takes advantage of the fact that light nuclei can have a strong contribution to neutron diffraction for determining the position of light atoms, notably deuterium, in crystal structures that also involve heavy elements. Neighbors in the periodic table are almost undistinguishable with X-rays, but they can have quite different scattering lengths for neutrons. This can be used to see such effects as ordering in Ni-Fe alloys. In this case, however, nature does not help much on its own, since the scattering lengths for natural Ni and Fe are again almost the same, and isotopically enriched Ni is required.

On the other hand, anomalous scattering, for which synchrotron radiation is beautifully suited, offers similar possibilities, with the added attractive feature of avoiding any extra work on the chemistry of the sample: it is "just" a matter of scanning in wavelength across well-chosen absorption edges.

As discussed in Chap. I, there is also a magnetic contribution,  $p$ , of the same order of magnitude as  $b$ , to the scattering amplitude of neutrons by atoms that have an electronic magnetic moment. The scattering length for magnetic scattering of neutrons involves a form factor that goes down with increasing  $\sin\theta/\lambda$ , just as for X-ray scattering, and for the same reason (the finite extent of the spatial distribution of the electrons). Magnetic X-ray scattering has developed too in the last few years. But the cross-sections are very small, it is still a tour de force to elucidate magnetic structures using X-rays, and neutrons remain the standard way of determining magnetic structures. Efficient use of the capabilities of both techniques often involves determining the underlying crystallographic structure with X-rays before going to a neutron source for the magnetic structure.

Since most elements contain various isotopes, with different neutron scattering lengths, a chemically pure sample behaves in neutron scattering as if it were made up of different species. This results in diffuse elastic scattering. Similarly, there is a term in the scattering amplitude related to the nuclear spin of the scatterer. Unless the nuclear spins are ordered (very difficult to achieve) and the neutrons polarized, this will also entail incoherent elastic neutron scattering. These incoherent elastic scattering effects, giving rise to background

Also, it is important to remember, as discussed in a striking manner in Chap. V, that even a normal laboratory X-ray generator produces X-ray beams with a much higher intensity than the neutron beams from a nuclear reactor, albeit in a small wavelength range. The ratio is huge when it comes to synchrotron radiation.

### VI.1.7. Beyond the kinematical approximation.

The standard expressions we have seen in this section are constantly used by structural crystallographers to relate the measured integrated intensities of Bragg reflections to the moduli squared of the structure factors of the various Bragg reflections. The kinematical approximation on which they are based looks wrong to a physicist, as it does not even take into account the conservation of energy, or of particles. Indeed neglecting the diffracted amplitude is not tenable when the crystal is perfect and not very small. This is why the next section is devoted to the dynamical theory. The kinematical approximation is nevertheless highly successful, and one of our challenges will be to understand why. We will return to this point in VI.3, after dealing with the dynamical theory of diffraction.

#### REFERENCES FOR VI.1.

- Bacon, G.E. (1975). Neutron Diffraction, 3rd edition. Clarendon Press.
- Cowley, J.M. (1981). Diffraction Physics. 2nd edition. North-Holland
- Giacovazzo, C., ed. (1985). Introduzione alla Cristallografia Moderna. Laterza, Bari
- Guinier, A. (1964). Théorie et technique de la radiocristallographie. Dunod.
- Hauptman, H.A. (1991). The phase problem of x-ray crystallography. Rep. Prog. Phys., 1427-1454
- International Tables for Crystallography: vol A (1987), vol C (1992). Published for the International Union of Crystallography by Kluwer Academic Publishers.
- McKie, D., McKie, C. (1986). Essentials of Crystallography. Blackwell.
- Schwartz, L.H., Cohen, J.B. (1987). Diffraction from Materials. 2nd edition. Springer
- Warren, B.E. (1969). X-ray Diffraction. Addison-Wesley.

## VI.2. Dynamical theory of diffraction

The dynamical theory of diffraction by a perfect crystal deals in a self-consistent way with the propagation of waves in a periodic structure. One of the key ideas is the fact that, if an incident wave can produce a diffracted one (Bragg's law or equivalent conditions satisfied), then the diffracted wave can be re-diffracted back into the incident wave direction. Thus the key concept is that of wave-fields, in which incident and diffracted wave are coupled.

Unlike the kinematical approximation, this theory of course satisfies the condition of conservation of energy or of particles.

We will go through the formal treatment, emphasizing the use of a particularly handy tool for understanding the behavior of wave-fields, the dispersion surface. More detailed expositions can be found in the references.

This treatment is really identical to that of energy bands in the weak potential approximation in solid state physics.

### VI.2.1. Propagation of a single wave, far from a Bragg reflection: refractive index

Whenever the characteristic Bragg-reflection effect of periodicity (in particular in crystals) does not come in, e.g. in visible-light optics, the use of a refractive index  $n$  is very handy. It is defined so that the wave-vector in vacuum,  $k$  and the wave-vector in the material  $k'$  are related by  $k' = n.k$ . In this description, simple transmission, the phase effects related to the positions of the scattering centers play no part at all. Accordingly, the refractive index is only related to mean values, such as the average density of scatterers or the average potential energy, and the fact that the material is crystallized or not (amorphous or liquid) makes no difference.

Useful expressions, as shown in I.4, are:

\* for X-rays:  $n = 1 - \frac{r_0 \lambda^2 \rho_0}{2\pi}$  where  $r_0$  is the classical electron radius ( $2.8 \cdot 10^{-15}$  m), and  $\rho_0$  is the mean electron density. For crystals  $\rho_0$  is no other than  $\sum_i n_i Z_i / V_C$ , where  $n_i$  is the number of atoms of type  $i$ , with atomic number  $Z_i$ , per unit cell of volume  $V_C$ . But  $Z_i$  is also  $f_{ai}(0)$ , the atomic scattering factor of atom  $i$  in the forward direction, or for scattering angle 0. We can write this, using the structure factor for X-rays (a number) associated with the 000 reciprocal lattice node  $F_0^x$  as

$$n = 1 - r_0 \lambda^2 \frac{\sum_i n_i f_{ai}(0)}{2\pi V_C} = 1 - \frac{r_0 \lambda^2 F_0^x}{2\pi V_C} = 1 - \frac{\chi_0}{2}$$

$$\sum_i n_i b_i$$

\* for neutrons:  $n = 1 - \lambda^2 \frac{\sum_i n_i b_i}{2\pi V_C}$ , the straightforward carry-over of the X-ray case, with  $b_i$ , the (nuclear) scattering length being the equivalent of the atomic scattering factor times the classical electron radius, as usual. Hence

$n = 1 - \lambda^2 F_0 / (2\pi V_C) = 1 - \chi_0 / 2$  again. Numerically,  $n$  is very close to 1, but slightly smaller both in the X-ray case and in most neutron cases (those where  $b > 0$ ).

This is enough to describe all the refraction, and possibly total reflection, effects at the boundary.

It has two important consequences. With  $n < 1$ , total external reflection is possible at an interface between vacuum and a material. This is the basis for neutron guide-tubes (discussed in 2.7), and for X-ray mirrors. Also we will have to describe a wave in a material by a wave-vector slightly smaller (in these usual cases) than in vacuum.

### VI.2.2. One Bragg reflection in a perfect single crystal

#### VI.2.2.1. Geometrical approach

As discussed in VI.1, a crystal is described by a periodic distribution in space of electron density  $\rho(r)$  (the relevant quantity for X-ray diffraction), or Fermi pseudo-potential  $V(r)$  (for neutrons). Hence  $\rho(r)$  can be written as a Fourier series, or, equivalently, as a plane wave expansion:

$$\rho(r) = \sum_h \rho_h e^{i \cdot 2\pi \cdot h \cdot r}$$

where the sum is over all reciprocal-lattice vectors  $h = ha^* + kb^* + lc^*$ . The  $\rho_h$  are very simply related to the structure factors characterizing each reciprocal lattice node  $h$  (we designate a node by the vector which points from the origin to this point),

$\rho_h = F_h / V_C$ , where  $V_C$  is the unit-cell volume.

The simplest description of diffraction in VI.1 led to Ewald's construction. We will henceforth use a slightly modified form. We draw two spheres with equal radii  $1/\lambda$ , centered at the origin of reciprocal space,  $O$ , and at the node  $H$  corresponding to  $h$ : then the tie-point corresponding to the common origin of  $k_0$  and  $k_h$  must be on the intersection of these spheres, as shown on fig. VI.4.

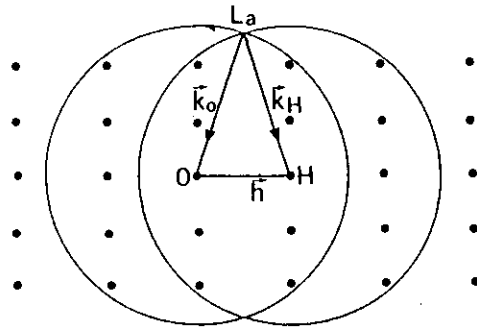


Fig. VI.4. — Modified form of Ewald's construction (see fig. VI.2 for the other form).

This is crude. The first improvement we must make is to take into account the refractive index. Since the waves in the crystal have slightly smaller wave-vector (except in the cases where  $b < 0$  for neutrons), we should draw two spheres each time, one for the waves in vacuum, the other for waves in the crystal (fig. VI.5).

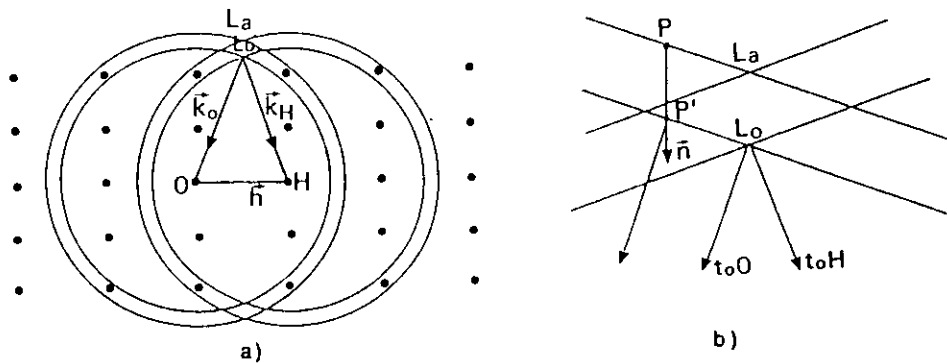


Fig. VI.5. — a. Effect of refractive index. The smaller spheres are associated with propagation in the crystal. The difference in radii is enormously exaggerated.

b. An enlarged view of the vicinity of the intersection of the spheres. Because of the magnification, the spheres are replaced by their tangents. Far enough from the Bragg condition, an incident wave with wave-vector  $PO$  in vacuum would generate in the crystal a wave with wave-vector  $P'O$ ,  $PP'$  being along the normal  $n$  to the crystal surface.

The intersection of the vacuum spheres is called the Laue point  $L_a$ , that of the crystal spheres is the Lorentz point  $L_o$ . Fig. VI.5b shows the neighborhood of

out in the next sub-section that the possible wave-fields in the crystal will be represented by points in the neighborhood of  $L_o$ .

We can already discuss the matching condition between the vacuum and the crystal waves: as in ordinary optics, continuity of the tangential component of the wave-vectors on the interface has to be assured. An incident wave in vacuum with wave-vector  $k_o$ , i.e. with origin  $P$  (its end must be  $O$ ) will generate in the crystal a wave with wave-vector represented by  $k'_o$ , a vector with its end still at  $O$  but with its origin at  $P'$ , the intersection of the perpendicular drawn from  $P$  to the interface. Fig. VI.5b shows the situation in reciprocal space. This is just a way of describing refraction.

Yet another, major, change will come in when we have discussed the propagation of waves near the Bragg condition in the crystal.

VI.2.2.2. Basic equations for possible wave-fields

We start out by discussing the wave-fields that satisfy the local conditions, viz. Schrödinger's equation for neutrons, or Maxwell's equations for X-rays, in the perfect crystal. The next step will be to discuss what wave-fields are excited by a given incident wave. The neutron case is simpler to start with than the X-ray case because we deal with a scalar wave, the De Broglie probability amplitude describing the neutron or neutron beam. Also, for nuclear scattering, the scatterers are point-like, hence, as discussed in Chap. I, the scattering length is independent of momentum transfer  $K$ .

We want our solution for the neutron wave-function to satisfy Schrödinger's equation in the crystal, with the (Fermi pseudo-) potential

$$V(r) = \frac{\hbar^2}{2\pi m} \sum_i b_i \delta(r-r_i).$$

$$\text{Hence } V_h = \frac{\hbar^2}{2\pi m V_c} \sum_i b_i e^{-2\pi i h \cdot r_i} = \frac{\hbar^2}{2\pi m V_c} F_h.$$

The solution we will try has the form suggested by Bloch's treatment of waves in crystals:

$\Psi(r) = u(r) e^{2\pi i k' \cdot r}$ , with  $u(r)$  a periodic function which therefore can be expanded into a Fourier series again:

$$u(r) = \sum_h u_h e^{2\pi i h \cdot r}, \text{ yielding } \Psi(r) = \sum_h u_h e^{2\pi i (k'+h) \cdot r}.$$

Let us look at the simplest situations. A single wave propagating in the crystal would be  $\Psi(r) = u_o e^{2\pi i k' \cdot r}$ , and  $u_o$  is just the amplitude of this single wave, with wave-vector  $k'$  in the crystal. If we take two components, we will have  $\Psi(r) = u_o e^{2\pi i k' \cdot r} + u_{h_1} e^{2\pi i (k'+h_1) \cdot r}$ : this just means that we have the incident wave plus a Bragg-diffracted wave with wave-vector  $(k'+h_1)$  and amplitude  $u_{h_1}$ . In usual terms, reflection  $h_1$  is excited. We know this will happen when the geometrical conditions for this Bragg reflection are approximately satisfied. This will be called a two-wave situation. It is easy, in

VI.1.2, more than two nodes of the reciprocal lattice would have to be near the Ewald sphere. In the present form, the tie-point would be near the intersection of spheres centered at O and at more than one other reciprocal lattice node.

In geometrical terms, we are looking for

- the locus of tie-points P' such that P'O = k', hence P'H necessarily k'+h, and
- the ratio of amplitudes u<sub>h</sub>/u<sub>0</sub> etc.

Now  $\Psi(r) = u(r) e^{2\pi i k' \cdot r}$  gives us

$$\Delta\Psi = - \sum_{\mathbf{h}} (k'+\mathbf{h})^2 u_{\mathbf{h}} e^{i(k'+\mathbf{h}) \cdot r}, \text{ whereas}$$

$$\nabla\Psi = \sum_{\mathbf{h}''} V_{\mathbf{h}''} e^{2\pi i \mathbf{h}'' \cdot r} \sum_{\mathbf{h}'} u_{\mathbf{h}'} e^{2\pi i (k'+\mathbf{h}') \cdot r} = \sum_{\mathbf{h}} \sum_{\mathbf{h}'} V_{\mathbf{h}-\mathbf{h}'} u_{\mathbf{h}'} e^{2\pi i (k'+\mathbf{h}) \cdot r}.$$

Schrödinger's equation thus reads

$$[(\hbar^2/2m)(k'+\mathbf{h})^2 - E] u_{\mathbf{h}} = - \sum_{\mathbf{h}'} V_{\mathbf{h}-\mathbf{h}'} u_{\mathbf{h}'}.$$

But  $E = (\hbar^2/2m) k^2$ , where k is the wave-vector in vacuo, and this energy is conserved since the scattering is assumed to be elastic. Hence

$$[(k'+\mathbf{h})^2 - k^2] u_{\mathbf{h}} = - \sum_{\mathbf{h}'} (2m/\hbar^2) V_{\mathbf{h}-\mathbf{h}'} u_{\mathbf{h}'} = - (4\pi/V_C) \sum_{\mathbf{h}'} F_{\mathbf{h}-\mathbf{h}'} u_{\mathbf{h}'}.$$

Or, if we adopt the notation  $(\lambda^2/\pi V_C) F_{\mathbf{h}} = \chi_{\mathbf{h}} = V_{\mathbf{h}}/E$ ,

$$\boxed{\frac{(k'+\mathbf{h})^2 - k^2}{k^2} u_{\mathbf{h}} = - \frac{\lambda^2}{\pi V_C} \sum_{\mathbf{h}'} F_{\mathbf{h}-\mathbf{h}'} u_{\mathbf{h}'} = - \sum_{\mathbf{h}'} \chi_{\mathbf{h}-\mathbf{h}'} u_{\mathbf{h}'}}$$

This is the fundamental equation of the dynamical theory of neutron diffraction.

It really represents an infinity of equations. But it is simpler than it looks. Note that the terms  $(\lambda^2/\pi V_C) F_{\mathbf{h}-\mathbf{h}'} = \chi_{\mathbf{h}-\mathbf{h}'}$  are very small, typically  $\approx 10^{-5}$ .

Let us continue concentrating on the two-wave case, with only the origin O and a specific node h<sub>1</sub> of the reciprocal lattice involved.

$$[(k^2 - k^2)/k^2] u_0 = - \sum_{\mathbf{h}'} \chi_{\mathbf{h}'} u_{\mathbf{h}'} = - [\chi_0 u_0 + \chi_{h_1} u_{h_1} + \dots]$$

$$[(k'+\mathbf{h}_1)^2 - k^2]/k^2 u_{h_1} = - \sum_{\mathbf{h}'} \chi_{\mathbf{h}_1-\mathbf{h}'} u_{\mathbf{h}'} = - [\chi_{h_1} u_0 + \chi_0 u_{h_1} + \dots].$$

This is consistent with the guess we made earlier: the second equation here can only be satisfied with u<sub>h<sub>1</sub></sub> not vanishingly small if (k'+h<sub>1</sub>)<sup>2</sup> is very near k<sup>2</sup>, hence if the tie-point is near the Laue and the Lorentz points, i.e. if the geometrical conditions for Bragg-reflection h<sub>1</sub> are nearly satisfied.

If they are not, then only u<sub>0</sub> is non-negligible, we are back in the one-wave case, but this gives us a condition on k'. It is easy to check that we recover exactly the expression for the refractive index given in VI.2.2.1, viz.  $n = 1 - \chi_0/2$ .

If they are, we have two equations with two unknowns, the amplitudes u<sub>0</sub> of the forward component and u<sub>h<sub>1</sub></sub> of the Bragg-diffracted component of the total wave-function in the crystal. We can have a non-trivial solution (non-zero amplitudes) only if the determinant of the set of equations is zero, and then we get the ratio of the amplitudes. We will now write, for convenience, k' = k'<sub>0</sub> since it is a vector ending on O, and similarly (k' + h<sub>1</sub>) = k'<sub>h</sub>. We will also quit using the subscript 1 which singles out the reciprocal-lattice node we are using.

$$\text{Then } (k'_0{}^2 - n^2 k^2) u_0 + \chi_{-h} k^2 u_h = 0$$

$$\chi_h k^2 u_0 + (k'_h{}^2 - n^2 k^2) u_h = 0,$$

which simplifies, since k'<sub>0</sub> and k'<sub>h</sub> are both close to nk, into

$$(k'_0 - nk) u_0 + k \chi_{-h} u_h / 2 = 0$$

$$(\chi_h k / 2) u_0 + (k'_h - nk) u_h = 0$$

whence the condition for existence:  $(k'_0 - nk)(k'_h - nk) - \chi_h \chi_{-h} k^2 / 4 = 0$ .

Setting  $(k'_0 - nk) = \xi_0$  and  $(k'_h - nk) = \xi_h$ , we thus have

$$\boxed{\xi_0 \xi_h = \frac{\chi_h \chi_{-h} k^2}{4} = \frac{|\chi_h|^2 k^2}{4} \quad \text{and} \quad \frac{u_h}{u_0} = \frac{2\xi_0}{k \chi_{-h}} = \frac{k \chi_h}{2\xi_h}}$$

### VI.2.2.3. Geometrical description: the dispersion surface

The first pair of equations have a simple geometrical meaning:  $\xi_0$  and  $\xi_h$  are the distances from a tie-point P' to the spheres with centers O and H and radii nk which describe propagation in the crystal in the one-wave (no Bragg diffraction) regime. The secular equation as transformed is the equation of a hyperbola, with asymptotes corresponding to the straight lines to which our approximation of fig. VI.5 has reduced the spheres that represent wave-vectors in the crystal but without Bragg diffraction (fig. VI.6). This two-branched hyperbola is called the dispersion surface. It contains full information about the waves that can propagate in the crystal. The pair of coupled waves making up  $\Psi$  is called a wave-field, Bloch wave, or Ewald wave.

Note that the figure is way out of scale: the distances to O and H should really be huge. The diameter S<sub>1</sub>S<sub>2</sub> of the hyperbola is easily found to be

$$S_1 S_2 = \frac{|\chi_h| k}{\cos \theta}. \text{ The larger the structure factor, the larger is this diameter.}$$

The amplitude ratio is proportional to the distance of the tie-point to the asymptotes: very near the H-sphere ( $\xi_h$  small), the wave-function is almost solely Bragg-diffracted type; near the O-sphere, it is almost solely forward wave, and near the apices of the hyperbola it involves equal forward and Bragg-

diffracted waves with equal amplitudes. Note how far this is from the kinematical approximation.

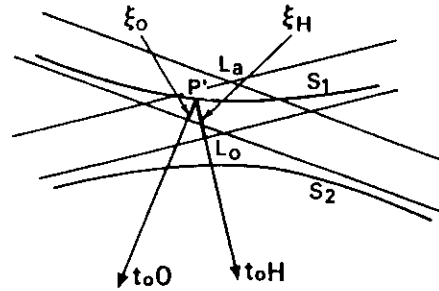


Fig. VI.6. — The dispersion surface as the locus of tie-points such as P' representing possible wave-fields.  $\xi_0$  and  $\xi_H$  are the distances from P' to the asymptotes, which are the tangents to the spheres with radius  $n/\lambda$  ( $n$ , the refractive index, is very close to 1). O and H are a kilometer or so away at the scale used.

The geometrical condition (Bragg diffraction corresponding to just the intersection of the two spheres, an unphysical result) has now matured into a gentle transition from an almost one-wave to a fully two-wave situation in the neighborhood of the Lorentz point  $L_0$ . Note that O- and H-waves play completely equal parts in this description.

The propagation direction, or direction of the probability current density, corresponding to a wave-field is the normal to the dispersion surface at the corresponding tie-point. This can be taken directly from the general result on constant-energy surfaces for (electron) states in solid state physics, as actually the dispersion surface is such a constant-energy surface. Near the asymptotes, propagation is along the one-wave directions, i.e. towards O and H. At the apices, it is just mid-way between the incident and the diffracted direction, i.e. along the lattice planes.

VI.2.2.4. Boundary conditions at the crystal entrance face

We now ask what wave-fields will really propagate in the crystal when a given incident plane wave hits the crystal surface. We have already looked at this question: the tangential component of the wave-vectors has to be conserved. The simplest case corresponds to an incoming plane wave.

Consider first the Laue (transmission) geometry (fig. VI.7), defined by the fact that the inward normal to the crystal surface lies between the incident beam and reflected beam directions. An incident wave represented by PO in vacuum and reflected beam directions...

surface, P'1 and P'2. One incident plane wave thus gives rise to two waves with forward character (those with wave-vectors P'1O and P'2O). From these, two waves with diffracted-wave character will be generated in the crystal.

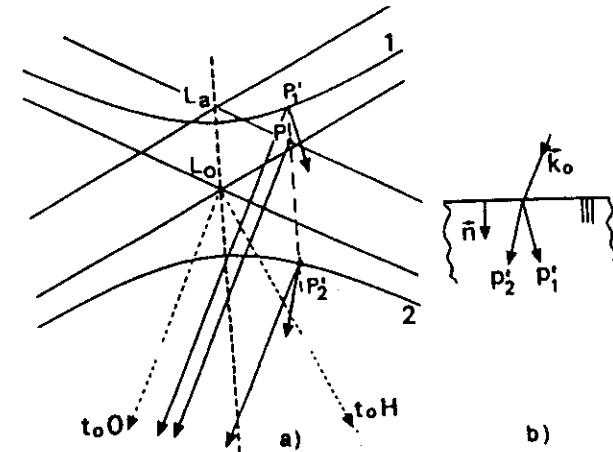


Fig. VI.7. — a. Laue (transmission) geometry. View in reciprocal space of the wave-fields, represented by tie-points P'1 and P'2, excited by an incident plane wave with wave-vector PO. Each wave-field consists of two waves, e.g. with wave-vectors P'1O and P'1H. The propagation directions of the two wave-fields, along the normals to the dispersion surface at P'1 and P'2, are different.

b. View in direct space of the propagation of the two wave-fields excited by one incident plane wave. Directions p'1 and p'2 correspond to tie-points P'1 and P'2.

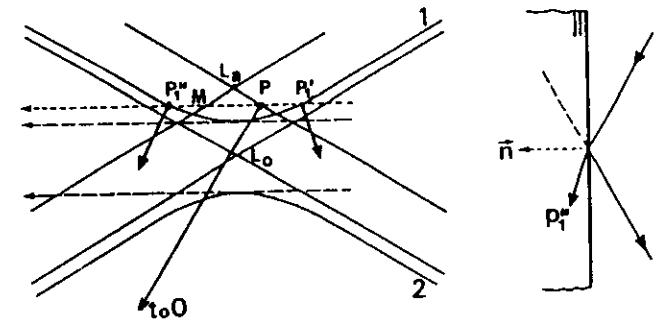


Fig. VI.8. — Bragg (reflection) geometry, otherwise same as fig. VI.7. Both possible wave-fields, associated to P'1 and P''1, are on the same branch of the dispersion surface. Only the one with propagation direction into the crystal, P'1, is physically acceptable for a very thick crystal.

Note that as the incident wave changes its incidence angle over a very small range (that corresponding to the really curved part of the dispersion

propagation angle by the very large angle  $2\theta$ , where  $\theta$  is the Bragg angle, several degrees. There is thus a huge angular amplification factor.

In Bragg (reflection) geometry (fig. VI.8), a simple conclusion appears for the limiting case when the crystal is infinitely thick. The two possible tie-points are on the same branch of the dispersion surface, and one of them would point out of the crystal. This is unphysical if there is no boundary within finite distance, hence only the wave-field corresponding to inward flow (tie-point  $P''_1$ ) will really be excited. A challenging situation is that of fig. VI.9, where no real tie-point is available since the normal to the entrance surface is between the two branches. Then the incident wave is totally reflected. The angular range over

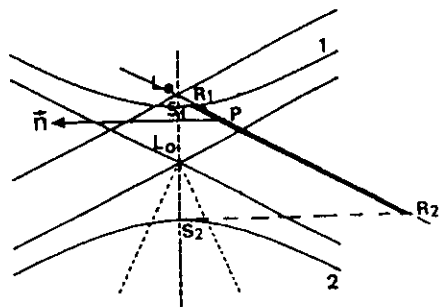


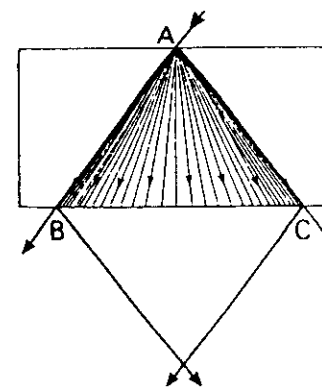
Fig. VI.9. — Bragg geometry. The total reflection range is  $R_1R_2$ .

which this happens is easy to find: in the symmetrical Bragg geometry, it is the angle between  $R_1O$  and  $R_2O$ . This is called the **Darwin width**,  $\epsilon = 2|\chi_h|/\sin 2\theta$ .

Note that the incident wave that excites the center of this total reflection range is not at the Laue point: the shift is just a refraction correction. Also the width of the total reflection regime changes if the geometry is asymmetric, i.e. if the crystal surface is no more parallel to the reflecting planes used. The angular width as well as the breadth of the totally reflected beam are then altered.

An interesting situation arises if the incident wave is sufficiently wide spatially that it can be considered as an almost plane wave, but sufficiently narrow that it corresponds to bundles of rays which can be traced. Then the different path directions associated with the excitation of regions of both sheets of the dispersion surface with very different propagation directions can be directly evidenced by the spatial positions, on the exit surface of the crystal, of the diffracted beams.

A very narrow beam can be treated as a coherent superposition of plane waves with a continuous range of wave-vectors and of amplitudes. If this range is larger than the Darwin width, it is convenient to approximate the incident beam by a spherical wave, as the range covered is enough to excite effectively the whole dispersion surface at once.



VI.10. — Spherical wave propagation. Wave-fields propagate throughout ABC, the Borrmann fan.

Then there will be wave-fields propagating in all directions between the incident and the diffracted direction, over the Borrmann fan ABC (fig. VI.10).

#### VI.2.2.5. Pendellösung effects

The interference effects between wave-fields are called Pendellösung effects for a reason which will appear in VI.2.2.7.

Consider first the plane-wave case. This implies that the incident beam is broad (strictly, it should be infinitely broad), and the two wave-fields excited will overlap throughout their propagation in the crystal (fig. VI.11). The O-type contributions are coherent, and their wave-vectors are  $P'_1O$  and  $P'_2O$  (fig. VI.7), which differ by  $P'_1P'_2$ , a small difference in wave-vector. The resulting probability current density therefore oscillates along  $P'_1P'_2$ , i.e. along the normal to the entrance surface, with period  $1/P'_1P'_2$  as the wave-fields propagate into the crystal.

The special case of symmetrical Laue geometry, and of an incident wave exactly at the Bragg setting, hence exciting  $S_1$  and  $S_2$ , corresponds to the longest period in direct space: this is called the **Pendellösung period**,  $\Lambda = 1/S_1S_2$ : at depth  $\Lambda/2$ , there is no O component any more, while it is maximum at depth 0,  $\Lambda$  etc.. Similarly for the H-type components, except that there is a phase difference initially: the combined amplitude for the H components is zero at the entrance surface, maximum at depth  $\Lambda/2$ , zero again for depth  $\Lambda$  etc. A rough order of magnitude for  $\Lambda$  is  $10 \mu\text{m}$ .

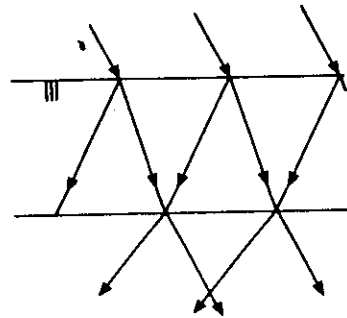


Fig. VI.11. — Pendellösung in plane wave case. Interference occurs over the area where wave-fields overlap.

Thus the equal-H (or O) -intensity loci are planes parallel to the entrance surface. If the exit surface is not parallel to the entrance surface, i.e. if the crystal is wedge-shaped, the diffracted intensity will oscillate as a function of distance from the edge.

In the narrow incident-beam case (spherical-wave approximation), only those wave-fields that propagate along the same direction do overlap over a long distance and can interfere. Thus interference occurs between wave-fields represented by tie-points that are symmetrically located with respect to the Lorentz point (fig. VI.12a), and there will be different periods ( $1/P'_1P'_4$ ) for different propagation directions. The equal-H-intensity loci can be shown to be hyperbolas, with asymptotes along the incident and diffracted beam directions (fig. VI.12b).

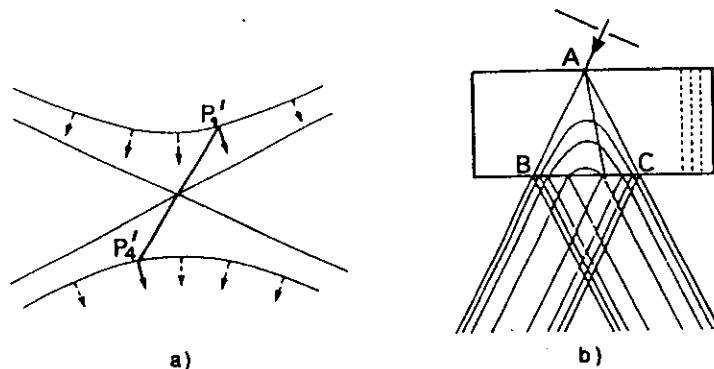


Fig. VI.12. — Pendellösung in spherical-wave case. a. View in reciprocal space: interference occurs between the wave-fields that have the same propagation direction, e.g. those represented by  $P'_1$  and  $P'_4$ .

b. View in direct space: equal-intensity surfaces.

The Pendellösung fringes are very sensitive to crystal distortion. This has been used in a variety of situations, e.g. to detect the effect of surface strains.

#### VI.2.2.6. The X-ray case, and the Borrmann effect

In the X-ray case, because the wave is vectorial, the two eigenpolarization modes, correspond to different scattering amplitudes. We saw in VI.1 that it is convenient to characterize them by a polarization coefficient  $C_i$  ( $C_\sigma = 1$  and  $C_\pi = \cos 2\theta$ ) multiplying  $F_h$  or  $\chi_h$ , and to deal with each polarization state separately, adding the intensities at the end. There are thus two hyperbolas (each with two branches) for the dispersion surface. The Darwin width is smaller, and the Pendellösung period longer, for  $\pi$ -polarization than for  $\sigma$ -polarization. There are therefore now four wave-fields for one unpolarized plane incident wave.

Also, absorption is no more negligible in most cases. This implies that  $\chi_h$  is complex whatever the choice of origin, and so are the wave-vectors. The presence of absorption makes anomalous transmission possible, and this is the Borrmann effect.

The two components of a wave-field are coherent, and their interference gives rise to a standing-wave pattern, with period  $1/OH$ , i.e. the lattice plane distance  $d_{hkl}$  of the excited Bragg reflection.

For the wave-fields with tie-point on branch 1 of the dispersion surface, the nodes can be shown to be on the lattice planes. The pattern is shifted by  $\pi$ , hence the antinodes are on the atomic planes, for the type 2 wave-fields.

Since absorption of X-rays involves the core electrons, and the intensity of the X-ray wave at their location, it becomes clear that type 2 wave-fields, whose intensity is consistently a maximum at the most active places in terms of absorption, will be very highly absorbed, while type 1 wave-fields will be less absorbed than without this modulation.

This is particularly true when the nodes become points of zero intensity. The two components must then have equal amplitudes, i.e. the wave-fields are represented by the apices of the hyperbola and propagate along the lattice planes used for the Bragg reflection. Actually, zero-intensity nodes also require that the electric field vectors be parallel, and this is only the case for  $\sigma$ -polarization. In thick crystals, where normal absorption would effectively kill transmission, the extra absorption of type-2 wave-fields makes no difference, but the anomalously high transmission of wave-field 1 provides a transmitted beam nevertheless. More precisely two beams come out: a diffracted one and a forward-diffracted one (fig. VI.13), both with  $\sigma$ -polarization. This is one way of getting polarized X-rays.

A similar effect exists for neutrons when the crystal has appreciable absorption. In either case, anomalous transmission is disrupted when the crystal perfection is disturbed, e.g. through vibrations.



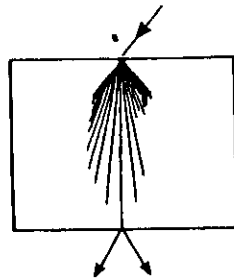


Fig. VI.13. -- Borrmann effect: only branch-1 wave-fields with propagation direction along the reflecting planes can survive in thick, absorbing crystal. They give rise to the forward-diffracted and diffracted beams.

#### VI.2.2.7. Ewald's analogy to coupled-pendula situation

P.P. Ewald offered a very nice analogy, which in fact gave Pendellösung its name (German for Pendular Solution): consider two identical pendula, somewhat coupled (through a spring on fig. VI.14), and damped as little as possible. Call one of them O, and the other H. If O is given an initial deviation and let go, it will oscillate, then lose amplitude, while H starts to move. After a while O stays at rest and H oscillates, and then the oscillation energy is swapped again.

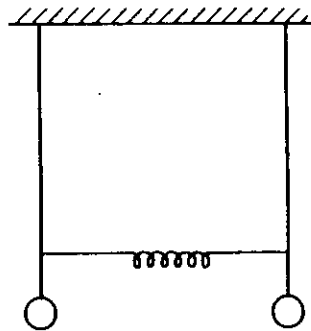


Fig. VI.14. -- Coupled pendula in Ewald's analogy to Pendellösung effect.

Time in the pendulum case corresponds to depth in the crystal diffraction situation. Both pendula can also be started together. A given oscillation mode will continue (it will be a stationary state) if both start with the same angle (symmetrical mode) or with opposite angles (antisymmetrical mode). In the latter case, the oscillation period will be different from that of either pendulum on its own. In the former case it will be the same, since the spring is not used at all. The situation corresponding to the symmetrical mode for the pendula is when the dispersion surface goes through the Laue point  $L_a$ , i.e. branch 1 of the

This analogy even shows which of the wave-fields can have decreased absorption. Let the two pendula be coupled by a spring and a damper (e.g. a cylinder with a viscous liquid, and a piston with little holes moving through the liquid): the damper would have no effect in the mode for which the wave vectors would be unaffected by the coupling, i.e. for tie-point  $L_a$ .

#### VI.2.2.8. Boundary conditions at the crystal exit surface.

The continuity condition again involves the tangential component of the wave-vectors and the amplitudes for the O- and H-waves.

In the plane-wave neutron case, the two diffracted-type waves share their combined amplitude, which depends on thickness (Pendellösung effect), between two H-type, diffracted outgoing waves in vacuum. These have practically the same wave-vectors, with their ends at H and their origins at the intersections with the sphere with center H and radius  $1/\lambda$  representing propagation in vacuum (a straight line in the region of interest) of the normals drawn through  $P'_1$  and  $P'_2$  to the exit surface. If the crystal is a flat plate (exit surface parallel to entrance surface), there is only one outgoing H-type wave. Similarly for the O-type, or forward-diffracted, wave(s). Note that the outgoing waves, in vacuum, all have, to within minute deviations, the direction of the incident and diffracted-wave directions corresponding to Bragg diffraction, irrespective of the propagation direction in the crystal of their parent wave-field.

In the almost-plane wave case, the path directions in the crystal will have separated if the crystal thickness is large enough, and the wave-fields will split independently into their O- and H- components.

In the spherical-wave situation, the emerging beams, both in the diffracted and in the forward-diffracted directions, will have the full width of the Borrmann fan.

The X-ray case involves separate treatment of the two polarization states.

#### VI.2.2.9. Rocking-curves and integrated reflectivity for perfect crystals.

A rocking-curve is the curve of diffracted intensity, scaled to incident intensity, versus the deviation of the incident wave from exact Bragg angle, or, more practical, versus crystal rotation angle  $\omega$ . Measuring it involves having a detector that is large enough to accept the whole diffracted beam. It also implies having a plane wave, which is not easy, and using a diffractometer with both the mechanical stability and the angular sensitivity needed to achieve reproducibility over a scale much smaller than an arc second. This is possible on very specially designed instruments operating preferably on high-brilliance sources.

When some of the above conditions are not fulfilled, a convolution of the rocking-curve with a usually broad instrumental function is obtained, and only the area under the rocking-curve can be reliably determined. This is the integrated reflectivity, or almost: we will call it  $R'_{hkl}$ . Actually the incident beam is measured by a number of photons or neutrons per unit time per unit area, and the diffracted beam is a number of photons or neutrons per unit time. Thus the

This is satisfied e.g. in the classical expression for the analogous situation in the kinematical approximation (small crystal with volume  $v$ , rotating-crystal method, neutron case):  $R_{hkl} = \lambda^3 |F_{hkl}|^2 \cdot v / (V_c^2 \cdot \sin 2\theta)$

Here, we idealize our problem with an incident plane wave (unrestricted), and will have to take into account the area of the incident beam intercepted by the crystal for comparison with the kinematical approximation.

**Bragg case**

The main feature of the Bragg case is apparent on the rocking-curve, as calculated in the zero-absorption limit which befits most situations in neutron diffraction, but not in the X-ray case (fig. VI.15 corresponds to an infinitely thick crystal): there is a region,  $\epsilon$  (the Darwin width) wide in angle, for which there is total reflection. On either side, reflection is partial, and the reflectivity decreases steadily with increasing deviation from Bragg's angle.

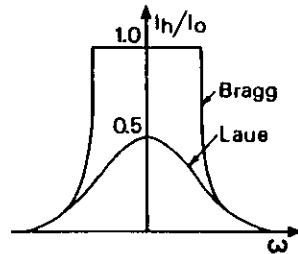


Fig. VI.15. — Laue and Bragg rocking-curves, averaged over oscillations, for perfect crystal, no absorption.

Clearly the area under the curve is slightly larger than  $\epsilon$ : the correct value, in the simple limit of an infinitely thick, non-absorbing crystal, and in symmetrical geometry, is  $R'_{hkl} = \pi \cdot \epsilon / 2 = \pi \chi_h / \sin 2\theta$ , which is very small. If the crystal is not infinitely thick, the reflectivity vs thickness curve, averaged over the Pendellösung oscillations, is expressed as

$$R'_{hkl} = \pi \chi_h \tanh A / \sin 2\theta, \text{ with } A = \pi t / \Lambda \text{ (fig. VI.16)}$$

**Laue case**

Here there is no total reflection, the reflectivity vs angle will strongly depend on crystal thickness (Pendellösung), but, when averaged over these oscillations, takes the form shown on fig. VI.15: the maximum reflectivity is 0.5.

Integration over the crystal rotation angle gives the curve shown on fig. VI.16, which corresponds, in symmetrical geometry, to the expression

32

$$W(A) = (\pi/2) \int_0^{2A} J_0(u) du, \text{ where } J_0(u) \text{ is the Bessel function of rank 0 and } A = \pi t / L.$$

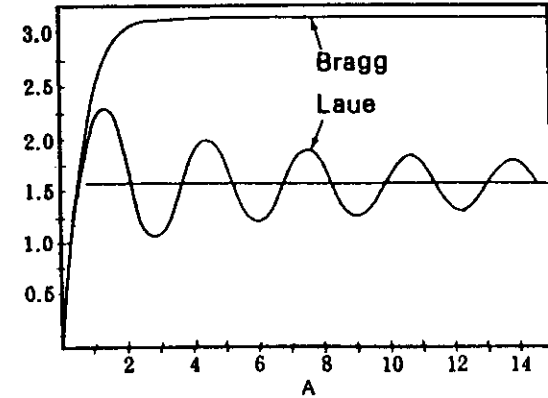


Fig. VI.16. — Integrated reflectivity  $R'_h$  vs  $A$  in Bragg and Laue case.

The initial slope of  $W(A)$  is  $\pi$ , and the limiting value of  $W(A)$  for large  $A$  is  $\pi/2$ .

The maxima and minima, when considered at fixed wavelength as a function of thickness, agree qualitatively with the discussion we made in the plane-wave case for exact Bragg-angle incidence, because this is the dominant term.

Note that the limiting value for thick, non-absorbing crystals, in symmetrical Laue geometry, is  $\pi \chi_h / (2 \sin 2\theta)$ . This is just half the value for the Bragg case.

**VI.2.3 Applications of dynamical theory**

Dynamical theory is necessary whenever diffraction by perfect crystals is involved. Thus it is involved in the design of monochromators, especially for synchrotron radiation, as described in Chap. III. It also made possible fascinating developments in experimental physics. Thus the very small angular width of rocking-curves for perfect crystals in non-dispersive, two-crystal settings has made it possible to investigate effects leading to very small broadening, i.e. very small-angle scattering. The fact that diffraction by a perfect crystal is a coherent process has led to the birth and growth of X-ray and neutron interferometry, where beams are split, then recombined, with applications ranging from basic experiments in quantum physics to measurements of scattering lengths. It is also involved in work on the surface diffraction techniques. In the area of structural crystallography, very accurate values of structure factors have been obtained from the Pendellösung effects using a variety of experimental setups. This is unfortunately restricted to very few crystals, viz. those that can be obtained in

imperfect crystals involving short-range distortions too, by a careful application of the best treatments of extinction, a problem which will be briefly discussed in VI.3.

The dynamical theory of diffraction by slightly imperfect crystals is the basis for X-ray topography (Chap. XVII).

#### VI.2.4. Omissions.

We have omitted several important points in this presentation, which was intended to give the essentials. In particular, we have restricted the explicit treatment to symmetrical geometries. It is easy to generalize this for moderate asymmetries, but some of the approximations made are not always valid in extreme cases. Also, the occurrence of multiple, or simultaneous, diffraction was dismissed: it is not as essential for X-rays and neutrons as for electron diffraction, but very promising developments for the direct measurement of the relative phases of different reflections are based on that principle (see Chang 1984).

### VI.3. The kinematical limit, and diffraction by crystals with intermediate perfection (extinction)

The assumption we used in VI.1 as the basis for the kinematical approximation, viz. crystal so small that any scattered amplitude be negligible, is valid whatever the crystal quality. We will show that indeed a perfect crystal diffracts according to the kinematical approximation if it is very small. We will also find that this condition is sufficient, but not necessary: the kinematical approximation can also be valid for larger crystals, provided they are bad enough. This is the key to its success in structural work, because in real crystals the periodicity is disturbed by various kinds of crystal defects. Indeed only rarely are crystals very good when they are of interest to structural crystallographers, i.e. when they have just been synthesized for the first time.

#### VI.3.1. The kinematical approximation as the limit of dynamical theory for a thin perfect crystal.

The dynamical expression for  $R'_{hkl}$  becomes, for symmetrical transmission geometry, in the thin (crystal thickness  $t \ll \Lambda$ ) perfect crystal regime:

$$R'_{hkl} = \frac{|\chi_h| \pi A}{\sin 2\theta} = \frac{|\chi_h| \pi^2 t}{\Lambda \sin 2\theta} = \frac{\lambda^3 |F_h|^2 t}{V_c^2 \cos \theta \sin 2\theta}$$

The area of the beam, coming in at an angle  $\theta$  to the normal to the surface, that covers an area  $S$  of the crystal is  $S \cos \theta$ . Hence  $R_{hkl} = \lambda^3 |F_h|^2 t S / (V_c^2 \sin 2\theta)$ . Since  $tS = v$  is the volume of the sample seen by the beam, this is exactly the kinematic expression.

Thus an ideally perfect crystal diffracts according to the kinematical approximation if its thickness is small compared to  $\Lambda$ . This can be seen graphically on fig. VI.16: kinematical behavior corresponds to the initial linear

But  $\Lambda$  involves the structure factor of the reflection used as well as the wavelength. For a given sample (thickness fixed) the condition for kinematical behavior is that the structure factor be small (weak reflection), and/or the wavelength be small (hot neutrons rather than cold ones;  $\gamma$ -rays rather than long-wavelength X-rays).

The physical meaning of the kinematical behavior of thin ideal crystals is that there is so little material that a diffracted wave has no chance of being re-diffracted into the incident direction, and that the amplitude diffracted out of the incident beam is negligible. We are thus back to the situation postulated in VI.1.1.

#### VI.3.2. The kinematical approximation as the bad crystal limit

The above argument can be extended, again neglecting absorption, to the situation where a crystal is subdivided into small units which diffract independently. This can be achieved if it consists of subgrains with linear dimensions  $\ll \Lambda$  (so that each satisfies the small crystal condition above) and misorientation larger than  $\epsilon$  between them (so that they could not diffract simultaneously the same part of a divergent monochromatic beam). Then the situation corresponds to the assumption of VI.1.1. as far as the integrated reflectivity is concerned. Any one subgrain sees the same incident beam intensity because no other subgrain upstream of it had the right orientation to diffract out appreciable amplitude, and there is negligible probability that another subgrain downstream should affect the diffracted beam from this subgrain. Thus *a bad enough crystal diffracts kinematically*. Here again  $\Lambda$  and  $\epsilon$  are involved, hence this behavior depends on wavelength and on the structure factor of the reflection used.

The kinematical limit can be approximated artificially for a given reflection from a good large crystal by imposing a curvature or a gradient of the lattice parameter such that the change in Bragg angle is about  $\epsilon$  for a path length  $\Lambda$ . This has been used in monochromator technology as a way of obtaining high reflectivity.

#### VI.3.3. Diffraction by imperfect crystals, extinction

The ideally perfect crystal case shows what the problem is, and why it is called extinction. When plotted versus crystal thickness, the integrated reflectivity starts out from 0, grows, and saturates. In the initial growth stage, the behavior is, as we saw above, identical with the kinematical approximation. But with larger thickness, the reflectivity is always less than predicted by the kinematical approximation, whence the term extinction, coined in reference to the kinematical limit.

The presence of extinction does not mean that the diffracted intensity is zero, i.e. that a reflection is absent. The absence of a reflection corresponds to the presence of screw axes, of glide planes in the space group of the crystal, or to the choice of a non-primitive unit cell. Unfortunately, these absences are called extinctions too, but the context should make the distinction clear.

Traditionally, extinction is characterized by an extinction coefficient  $\gamma$  defined as the ratio of the observed integrated intensity over that given by the

kinematical approximation. Thus, unfortunately again, strong (large) extinction effects correspond to small  $\gamma$ . The behavior of perfect crystals (dynamical diffraction) then corresponds to very small values of  $\gamma$  when the thickness is large.

#### Almost perfect crystal

In this case, the reference should be the perfect crystal, for which the behavior is well understood through the simplest form of dynamical theory, as discussed in section VI.2. The effect of departures from perfection is then usually to increase the diffracted intensity, hence to reduce extinction. This can be apprehended simply by remembering that, in a perfect crystal, a monochromatic, but non-parallel, beam would have only a tiny part, roughly the Darwin width  $\epsilon$ , diffracted. Any region in the crystal where the distortion leads to a change in Bragg condition of the order of  $\epsilon$  or larger will diffract a new part of the beam, hence provide extra diffracted intensity. This ceases being true only in the extreme limit of a thick absorbing crystal, where the Borrmann effect provides a diffracted beam if the crystal is perfect, and where deviations from perfection disrupt this anomalous transmission effect. In the ideally imperfect crystal,  $\gamma = 1$ , i.e. there is no extinction.

The almost perfect crystal situation includes two very different aspects. Perfect crystals (mainly silicon) can be intentionally deformed elastically, or submitted to a temperature gradient, or strained by a surface layer such as oxide, and the distribution of diffracted intensity on the exit surface as well as the rocking-curves or at least integrated reflectivities measured.

On the other hand, very good crystals usually include some defects, such as dislocations, whose elastic behavior, at large enough distances from the core, is well known. Each of these defects affects wave-field propagation. The distribution of diffracted intensity across the diffracted beam, when recorded on a photographic detector, provides an image (or topograph, see Chap. XVII), where the defects are visible because of their effect on the wave-fields. Intricate effects, leading in particular to beautiful images, are observed. They can be understood in terms of the changes in wave-field propagation and interference due to the long-range strain field around the defects. As a result, the characteristics of individual defects, e.g. the direction, magnitude and sense of the Burgers' vector of dislocations, can be fully determined.

Much effort has gone, with considerable success, into understanding, qualitatively and analytically, these effects in comparatively simple circumstances. The computer calculation of wave-field propagation in a distorted crystal and the simulation of topographs are also well developed, using the Takagi-Taupin equations. This is outside the scope of this section.

#### Statistically distorted crystals: the extinction problem

Seen from the point of view of structural crystallographers, extinction is a nuisance because it destroys the simple relationship between measured intensities and the moduli squared of the structure factors. Detecting extinction

dependent, and a good way of detecting it is to measure the reflectivity at different wavelengths. It is also worse for strong reflections, and structural crystallographers sometimes go around the problem by just ignoring the strongest reflections in their data sets. In practice, extinction is an important problem for neutron rather than for X-ray diffractionists, because the weak neutron fluxes available make it necessary to work under conditions yielding higher integrated reflectivities, hence to go to higher values of  $t/\Lambda$  by using large samples. The fight against extinction can involve cold-working the sample if it is a metal, or even more brutal treatments like dropping it into liquid nitrogen.

The crystals used for structural work usually contain quite a high density of crystal defects. It would therefore be usually impossible, as well as completely devoid of interest to the users, to make an observation of the actual individual defects. The defect distribution in a crystal must then be characterized by only few parameters, and a statistical approach must be used for extinction correction.

The older literature on extinction is based on the concept of the mosaic crystal and distinguishes primary and secondary extinction. Primary extinction corresponds to mosaic blocks that are too large, and where individual blocks already diffract less than in the kinematical approximation. Secondary extinction is related to the misorientation distribution being too narrow (Zachariassen, 1945). The accepted procedure is Becker and Coppens's treatment, which works very well for moderate extinction and is incorporated in structure determination computer packages. However, it cannot reproduce the behavior of perfect crystals, characterized e.g. by Pendellösung oscillations, as a limit, because it is based on intensity transfer equations and does not take into account the possibility of interference.

It is now apparent that the mosaic model is unrealistic. The newer treatments try to describe extinction as a whole, and some of them attempt to cover the whole gamut of possibilities, from the ideally perfect crystal to the ideally imperfect, kinematical one. Work is continuing in this difficult area.

#### REFERENCES FOR VI.2. AND VI.3.

- Authier, A. (1970), in *Advances in structure research by diffraction methods*, ed. by R. Brill, R. Mason. Pergamon. Also in *Modern diffraction and imaging techniques in material science*, edited by S. Amelinckx, R. Gevers, G. Remaut, J. Van Landuyt, pp. 481-520. North Holland.
- Batterman, B.W., Cole, H. (1964): *Revs. Mod. Phys.*, **36**, 681-717
- Chang, Shih-Lin (1984). *Multiple diffraction of X-rays in crystals*. Springer.
- International Summer School on X-ray Dynamical Theory and Topography, Limoges, France, August 1975. Edited by F. Balibar (unpublished)
- International Tables for Crystallography: vol A (1987), vol C (1992), published for

Vol. B will contain a Chapter on Dynamical Theory of X-ray Diffraction by A. Authier.

Kato, N. (1974), in X-ray diffraction. L.V. Azaroff, editor. McGraw-Hill.

Pinsker, Z.G. (1978). Dynamical scattering of X-rays in crystals. Springer.

Schwartz, L.H., Cohen, J.B. (1987): Diffraction from Materials, 2nd edition, Springer.

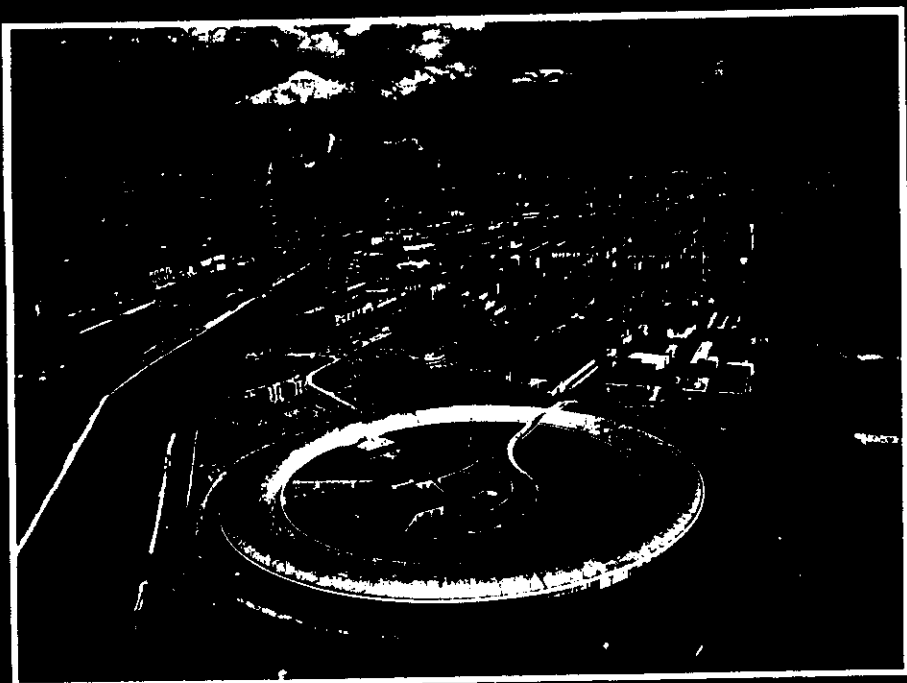
Zachariasen, W.H. (1945): Theory of X-ray diffraction in crystals. Wiley.  
Reprinted by Dover Publications, 1967.

Additional material to the lecture

“Specific optical elements for a XAS beam line”

by Hélio Tolentino

# NEUTRON AND SYNCHROTRON RADIATION FOR CONDENSED MATTER STUDIES



HERCULES

## CHAPTER III

### X-RAY OPTICS FOR SYNCHROTRON RADIATION

A. FREUND

#### III.1. Introduction

About 100 years ago in his original work C.W. Röntgen after having discovered the X-rays was unable to detect any deflection of X-rays by lenses and concluded that there should be no refraction of X-rays by matter or that at least such effects should be very small. Later specular reflection of X-rays by surfaces was observed and early in this century Max von Laue and coworkers discovered X-ray diffraction by single crystals and developed the dynamical diffraction theory by perfect crystals. This was the beginning of X-ray optics, and the underlying principles of this *Bragg-optics* are still valid today. They were at the origin of much work carried out on X-ray monochromators used in conjunction with X-ray tubes that have become standard equipment of today's X-ray instrumentation. A review of these techniques can be found in the International Tables for Crystallography (1968).

With the advent of synchrotron radiation sources and their specific properties, in particular the energy tunability and the high brilliance of modern high energy synchrotron storage ring facilities (ESRF, Grenoble, France; APS, Chicago, USA; SPring 8, Harima, Japan), it became necessary to revise this optics drastically. Mirrors play now a very important role and a new type of optical element called layered synthetic microstructures or, briefly, multilayers were added to the instrumentarium of state-of-the-art X-ray optics. Several reviews on this topic show the transition from conventional to completely new schemes (Matsushita and Hashizume, 1983; Caciuffo et al., 1987; Freund, 1989; Batterman and Bilderback, 1991; Malgrange, 1992). They are all necessarily incomplete because the field is very wide and in steady development. The limited space will make this article even less complete so that, in addition to the above papers, the interested reader is referred to more specialized recent work published regularly in the proceedings of synchrotron radiation instrumentation conferences (SRI, the most recent ones appeared in Rev. Sci. Instrum. 63, 1992) or the relevant volumes of SPIE proceedings.

#### III.2. Role of X-ray optics

An optical system is composed of a source emitting a beam and of optical elements that transform this beam downstream till the sample under study and to the following detector. When choosing the optical system of such a beamline it is therefore important to consider the source characteristics as well as the kind of detector to be used, too. The task of the optics is to transform the beam in such a way as to match it ideally to the experiment. The intensity *versus* resolution (energy, angle, space) optimization implied in this procedure has to take into

account not only the reflection properties of mirrors, crystals and multilayers, but also the consequences of the very high heat load produced by wigglers and undulators inserted in the straight sections of electron storage rings and the behaviour of optical devices under high X-ray power. A very clear demonstration of such a complete optimization was given recently by Wulff (1992).

The beam transformation is governed by Liouville's theorem that states that the particle (photon) phase space density can never be increased if conservative forces are applied to the system. Ideal optical elements would totally conserve both emittance (phase space volume) and brilliance (phase space density). On the other hand, there are always losses associated with the limited efficiency of optical devices so that the ideal optics would be no optics at all. At least, the number of elements should be minimized. Losses of beam quality and photon quantity arise from fundamental limits (aberrations, diffraction effects at slits...) and from technological limits (mirror surface roughness, slope errors, crystal imperfections...) and materials problems are of major importance in the research and development of X-ray optics. In addition to conservation of emittance and brilliance the optics should produce a "clean" beam, i.e. free of background radiation, harmonics, glitches (parasitic reflections) and other beam contaminations that can deteriorate the quality of an experiment.

In order to optimize the design of a beamline one has to know both the detailed phase space properties of presently available beam-defining devices and of their combined effect on the X-ray beam. There are several kinds of graphic schemes in real, reciprocal and phase space that can be used to estimate the global beamline performance and to find out the best matching between the elements (DuMond, 1937; Davis, 1990; Matsushita and Kaminaga, 1980; Suortti and Freund, 1989). This first approach is then completed by a more precise and quantitative ray-tracing that approach veritable computer simulations of X-ray scattering experiments (Lai et al. 1988, Sanchez del Rio, 1992).

The criteria for suitable X-ray optics materials and devices can be summarized as follows:

- i) Ability to reflect photons of a desired energy range at a suitable angle.
- ii) Resolution in space, angle and energy matched to the experiment.
- iii) Energy tunability within a specified range.
- iv) Maximum X-ray transmissivity inside the domains defined by i) and ii) and the range chosen in iii), and very low transmissivity outside these ranges.
- v) Focusing possibilities should almost always be provided.
- vi) Excellent performance under severe radiation and heat load (materials problems).
- vii) Availability in sufficient size and quality at a reasonable price.
- viii) Ease in preparation and mounting (machinability, polishability).
- ix) High degree of flexibility.
- x) Supports of high mechanical precision, stability and reproducibility.

It is clear that the fulfilment of all these requirements is a matter of a best compromise, i.e. of an optimization in the space of *dreams and reality*:

For example, present ESRF specifications for more than 1 m long mirrors are a microroughness of about 0.1 nm rms and a slope error of 1  $\mu$ rad, the latter corresponding to the angular stability of an undulator beam. The same angular

positioning precision and stability holds for single crystal monochromators although in some cases this can be relaxed so that not only highly perfect crystals but also mosaic or otherwise non-perfect crystals are sometimes suitable as monochromators. Without giving details about the specific needs of the various types of experiments it should be mentioned that the beam cross-section at the sample ranges from 1  $\mu$ m<sup>2</sup> or less (microprobe) up to 10 cm<sup>2</sup> (topography), the angular resolution varies between 1  $\mu$ rad or even less (plane wave topography) and 10 mrad (microprobe), and the relative energy resolution required is between 10<sup>-7</sup> (phonon scattering) and 0.1 (microscopy). The energy (wavelength) range to be covered is from about 0.3 keV (40 Å) up to a few hundred keV (a few hundredth of an Å). These very wide ranges need a wide range of optics that, in addition, will be exposed to very intense beams: at the ESRF the first optical element has to withstand an X-ray power of up to several kW at a power density of up to 100 W/mm<sup>2</sup> (see Freund et al., 1990). Many materials are then eliminated, stability becomes a major issue, many new engineering problems arise, precise facilities for testing the performance of optical elements need to be developed and new approaches have to be sought such as cryogenic cooling and active and adaptive optics (Freund, 1992a).

### III.3. Optical elements for synchrotron X-rays

Table 1 lists the various devices presently used for X-ray beam conditioning and the energy ranges for which they are most efficient. These ranges are determined by fundamental and technological limitations. For instance, a single crystal monochromator cannot reflect X-rays of wavelength longer than twice the d-spacing of its lattice planes. Conversely, the improvement of multilayer preparation techniques could allow their application to higher X-ray energies.

	Devices for Beam Definition	Soft X-rays 0.3-3 keV (40-4 Å)		X-rays 3-30 keV (4-0.4 Å)		Hard X-rays 30-300 keV (0.4-0.04 Å)		Beam Parameters
		R	T	R	T	R	T	
Beam Shapers	Pinholes, Diaphragms	xxx		xxx		xxx		$\psi$ , $\Delta x$
	Soller Slits		x	xxx		xxx		$\psi$
Total Reflection	Mirrors	xxx		xxx				$\psi$ , $\Delta x$ , (E, $\Delta E$ )
	Guide Tubes		x	x				$\psi$ , ( $\Delta x$ , E, $\Delta E$ )
Linear and Planar Microstructures	Gratings	xxx	xx	x				$\psi$ , $\Delta x$ , E, $\Delta E$
	Fresnel Plates	xx	xx	x				$\psi$ , $\Delta x$ , E, $\Delta E$
Bragg Optics	Multilayers	xxx	x	xx	x			$\psi$ , $\Delta x$ , E, $\Delta E$
	Single Crystals	x		xxx	xx	x	xxx	$\psi$ , $\Delta x$ , E, $\Delta E$ , P
Combined Systems	Multilayer Gratings	x		x (?)		x (?)		$\psi$ , $\Delta x$ , E, $\Delta E$
	Bragg-Fresnel-Optics	x (?)		x (?)		x (?)		$\psi$ , $\Delta x$ , E, $\Delta E$ , P

Table 1.- X-ray optical devices (presently existing or under development), the energy and wavelength ranges where they are applied (R-reflection, T-transmission geometry). Use: xxx-frequently, xx-moderately, x-occasionally, ? - maybe, and the beam parameters which they define (to some extent):  $\psi$ -divergence,  $\Delta x$ -spatial resolution, E-energy,  $\Delta E$ -energy spread, P-polarization.

The most ordinary device is a slit, which may be of quite simple construction when used to eliminate stray radiation, but which becomes a huge beam shaper consisting of up to one meter long water-cooled copper jaws used in



grazing incidence to limit the size of powerful wiggler beams. At the other extreme, it is not easy to fabricate very narrow pinholes of submicron diameter, for example, for microbeam experiments. Here the discussion will focus on the following devices: mirrors, monochromators and multilayers. The latter, also called layered synthetic microstructures, are sometimes referred to as "multilayer mirrors", sometimes as "multilayer monochromators", and are thus situated between single-layer mirrors and the three-dimensional lattices of single crystal monochromators. If they have a gradient of the layer thickness perpendicular to the surface they do not show distinct Bragg peaks but an increase of the total reflection range ("super-mirrors"). Because gratings are not very efficient at medium and higher X-ray energies they will not be described here. The same holds for Fresnel lenses. Fig. III.1 shows the energy and wavelength dependence on the glancing angle and the typical ranges covered by the three major kinds of beam-defining devices. These "DuMond diagrams" are based on Snell's law for mirrors and on Bragg's law for single crystals and multilayers. At a given glancing angle, mirrors reflect X-rays of all energies smaller than the critical energy characteristic of a given material (hatched area), whereas single crystals and multilayers select sets of narrower or wider energy bands corresponding to Bragg reflections and their harmonics (double curves, see insert). The synchrotron beam divergence can be shown as a horizontal segment in this diagram. It varies from about 30  $\mu$ rad (undulators) to 300  $\mu$ rad (wiggles) and depends on energy (Freund et al., 1990).

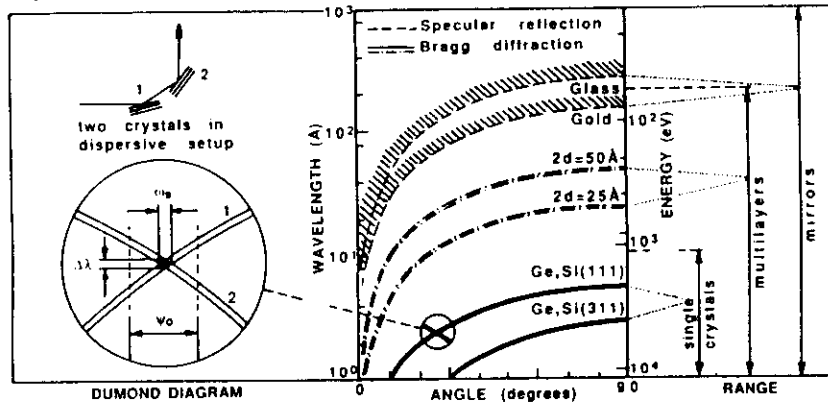


Fig. III.1.- The relation between the angle of reflection and the X-ray wavelength and energy for three major kinds of beam defining devices.

According to the experimental requirements, one or more of these optical devices can be used in flat or focusing geometries. Their combined effect on beam transformation and thus their optimum sequence can also be determined with the help of the DuMond or other graphic schemes. As an example, the successive reflections of a beam by two crystals in the dispersive mode (same sense of beam deflection) is shown to produce a beam whose divergence is equal to the intrinsic "Darwin" width,  $\omega$ , of the crystals and whose energy bandwidth  $\Delta E/E = \omega \cot \theta_0$  is thus independent of the white beam divergence,  $\phi_0$  (see the insert of Fig. III.1).

### III.4. X-ray mirrors

X-ray mirrors are nowadays widely applied as high energy cut-off filters and as focusing devices. They can reduce the power load on the more delicate single crystal monochromator following downstream by typically a factor two. They have the advantage that the heat and radiation is spread over a much bigger surface than in the case of crystals because the reflection angle is very small, usually of the order of some mrad. Specular reflection from real (non-ideal) surfaces is based on a modified Fresnel theory that takes into account surface roughness ("finish") and slope errors ("figure"). Both can be measured by visible light interferometry and the results are expressed in terms of a power spectral density function involving a Fourier analysis of the surface height variation as a function of spatial frequency. This is then used by a formalism calculating the X-ray reflection properties for different energies (Takacs, 1986). The requirements for ESRF mirrors were described by Freund et al. (1990).

Specular reflection is related to the index of refraction,  $\eta$ , given in the X-ray regime by Parrat (1954):

$$\eta = 1 - \delta - i\beta \quad (III.1)$$

$$\text{where} \quad \delta = r_0 N_0 \rho / 2\pi A (Z + \Delta f) \lambda^2 \quad (III.2)$$

$$\text{and} \quad \beta = \lambda \mu / 4\pi. \quad (III.3)$$

The decrement in the index of refraction,  $\delta$ , is small, of order  $10^{-5} - 10^{-6}$ . The imaginary part of  $\eta$  is proportional to the linear absorption coefficient,  $\mu$ . The classical electron radius  $r_0 = e^2/mc^2$  is  $2.82 \times 10^{-13}$  cm,  $N_0$  is the Avogadro number,  $\rho$  the density of the material,  $A$  the atomic weight and  $\lambda$  the X-ray wavelength ( $= 12.4/E$  in  $\text{\AA}$  if the energy  $E$  is in keV). The term  $(Z + \Delta f)$  is the real part of the scattering factor in forward direction consisting of the atomic number,  $Z$ , and of the dispersion correction,  $\Delta f$ . The critical angle of reflection is  $\theta_c = (2\delta)^{1/2}$ . At angles below or equal to  $\theta_c$  X-rays are reflected whereas above they are absorbed by the material. For low  $Z$  materials a good approximation is:

$$\theta_c \text{ (mrad)} = 1.6 \lambda \text{ (\AA)} (\rho \text{ [g/cm}^3])^{1/2} \quad (III.4)$$

in the absence of absorption edges. Another practical expression for the critical angle is good to within 10%:

$$\theta_c E \text{ [keV]} = 33 \text{ keV mrad for low-Z surfaces} \quad (III.5)$$

$$\text{and} \quad \theta_c E \text{ [keV]} = 77 \text{ keV mrad for high-Z surfaces.} \quad (III.6)$$

At ESRF mirrors are used up to an energy of 30 keV. With a beam height of 3.5 mm (wiggler source) and a platinum coated surface ( $\theta_c = 2.6$  mrad) the mirror length becomes 1.4 m. This is a typical number for modern synchrotron hard X-ray mirrors. The mirror reflectivity  $r$  as a function of angle (energy) is a step function the step occurring at the critical angle (energy). This means that for a given angle X-rays of all energies up to a critical energy  $E_c$  are reflected whereas higher energies are absorbed (filter effect). The step function is smeared by absorption and can be described by:

$$r = [h - q \{2(h-1)\}^{1/2}] / [h + q \{2(h-1)\}^{1/2}] \quad (III.7)$$

$$\text{where} \quad h = q^2 + [(q^2 - 1)^2 + (\beta/\delta)^2]^{1/2} \quad (III.8)$$

and  $\theta' = \theta/\theta_c$ . Because  $\theta$  is proportional to  $1/E$  equations (III.7) and (III.8) can be written in terms of energy by replacing  $\theta$  by  $1/E$  where  $E' = 1/E_c$ . A set of such curves observed on a glass mirror coated with 50 nm of platinum are shown in Fig. III.2. The wiggles are due to multiple reflections inside the thin Pt layer (Kiessig fringes).

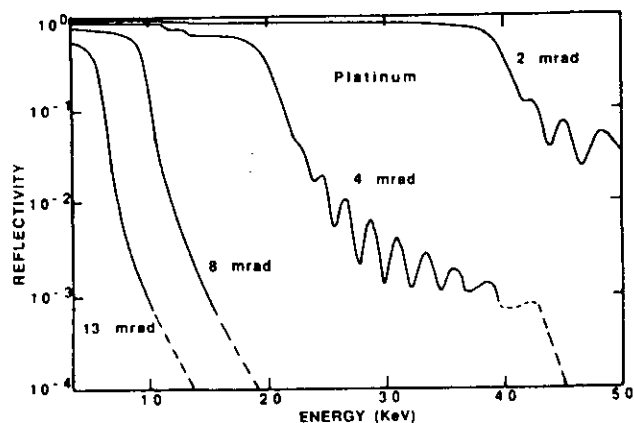


Fig. III.2.- Reflectivity of a platinum coated glass mirror at different glancing angles. (After Bilderback and Hubbard, 1982).

The most important application of mirrors is to focus an X-ray beam onto the sample. The efficiency of the focusing is determined by aberrations and by mirror imperfections such as microroughness and slope errors. The best conditions are obtained with an elliptical or parabolic shape of the mirror surface. Because of easier preparation they are often approximated by spheres or cylinders with circular cross section. Then spherical aberration effects occur that increase with decreasing angle and with increasing magnification. The relations between the various parameters of the focusing geometry are:

$$R_m = 2pq/(p + q) \sin\theta \quad (\text{III.9})$$

for meridional (in-plane) focusing (radius  $R_m$ ) and

$$R_s = 2pq \sin\theta/(p + q) = R_m \sin^2\theta \quad (\text{III.10})$$

for sagittal (out-of-plane) focusing (radius  $R_s$ ), where  $p$  and  $q$  are the source-to-mirror and mirror-to-sample distances, respectively.  $R_m$  is typically  $\sim 10$  cm whereas  $R_s$  is  $\sim 10$  cm.

For double focusing toroidal mirrors are used which can be manufactured by grinding a cylinder of radius  $R_s$  into a substrate which is subsequently bent to a radius  $R_m$ . The bending corresponds to a deflection of typically 20  $\mu\text{m}$  at the centre which shows the high precision needed for mirror preparation techniques and supports. Benders are very useful also for varying the radius of curvature when changing the glancing angle, at least in meridional direction, and for correcting deformation arising from gravitation and thermal load. High figure

accuracy and small surface roughness are difficult to achieve at the same time. The best results recently reported are slope errors of about 5  $\mu\text{rad}$  rms and a roughness of 1  $\text{\AA}$  rms for superpolished surfaces. This means that for  $q = 10$  m the focus will be broadened by about 0.1 mm which is about equal to the source size of modern storage ring facilities. In all cases a best compromise has to be found between aberrations, manufacturing tolerances and the precision of the supports.

When the mirror is used as the first optical element in the beamline, problems related to radiation damage and thermal gradients are added to manufacturing difficulties. High-power wigglers yield a total power of several kW and power densities up to a few 100  $\text{W}/\text{mm}^2$  perpendicular to the beam. Gradients parallel and perpendicular to the surface create strains which deform the surface and degrade the mirror performance even if they are cooled. A substantial part of the radiation is absorbed by the mirror and gives rise to radiation damage. Here materials problems become very important (see section III.7) and only a few materials remain under consideration: Si, SiC, "Glidcop" (a Cu- $\text{Al}_2\text{O}_3$  alloy). For post-monochromator mirrors Zerodur and ULE (ultra-low expansion) as well as fused quartz are commonly used that have excellent mechanical properties (stiffness, hardness) and are easier to polish.

Adaptive mirror technology is currently being developed at the ESRF (Susini, 1992) where the thermal deformation is counterbalanced by a mechanical deformation of the mirror surface by means of piezo-electric actuators attached to the back of the mirror body. The surface shape is continuously surveyed in-situ by an optical system connected to a servo-loop that maintains the surface constantly in the desired shape even if the perturbations (heat load, etc.) change with time. With this technique any kind of surface shape can be achieved, and even manufacturing slope errors can be corrected to some extent.

### III.5. Single crystal monochromators

Perfect single crystals are generally used to select a more or less narrow monochromatic energy band out of wiggler or undulator radiation according to Bragg's law:

$$2 d_{nh} \sin\theta_b = \lambda/n \quad (\text{III.11})$$

where  $d_h$  is the lattice spacing of crystallographic planes belonging to the reflection,  $h$  stands for the Miller indices and  $\theta_b$  is the Bragg angle given by the angle between the incident (or the reflected) beam and the lattice planes. The integer  $n$  denotes the reflection order:  $d_{nh} = d_h/n$  and thus wavelengths  $\lambda_1, \lambda_1/2, \lambda_1/3, \dots, \lambda_1/n$  are reflected simultaneously as far as the reflections are not forbidden by the crystalline structure. Crystals can be used in reflection ("Bragg case") or in transmission geometry ("Laue case"), and the reflection can be symmetric or asymmetric (see the insert in Fig. III.3). In all cases except the symmetric Laue case the reflection occurs at an angle different from that given in Eq. (III.11) because of refraction. This correction is quite small, of the order of the width of the reflection curve, also called Darwin width. This width can be considered as the result of the finite penetration depth of the X-rays into the crystal, called the extinction depth,  $t_c$ , that is due to the fact that at each lattice plane a small portion of the beam is reflected out of the incident beam. Usually, this depth is much smaller than the absorption depth,  $t_a$  (see Table III.2). Thus a

crystal can be compared to a grating and the Darwin width to the width of the corresponding interference pattern. In fact, the diffraction process inside a perfect crystal is a little more complex. The dynamical theory describing it can be found in textbooks, for instance in Zachariasen (1945), or in a condensed form by Schlenker in this book (Ch. VI). Here I will give just a few results for the Bragg case. Fig. III.3 shows a set of diffraction patterns for  $\sigma$ -polarization corresponding to four reflection orders from the (220) planes of a "thick" ( $t \gg t_c$ ), perfect silicon crystal where the first order wavelength is 1.54 Å. From the shape of the curve it is clear that there is a range of total reflection where the reflectivity is 1 (broken line, without absorption), and then the intensity is decreasing according to  $\Delta^{-2}$  as in the case of specular reflection by mirror surfaces (where  $\Delta = \theta - \theta_b$  is the deviation from the Bragg angle). Another similarity to the mirror case is the smearing of the step function by absorption. The asymmetry is due to the fact that the maximum of the standing wave amplitudes inside the crystal are located *between* the atomic layers on the left side ( $\rightarrow$  minimum absorption) and *at* the atomic layers on the right side ( $\rightarrow$  maximum absorption), respectively.

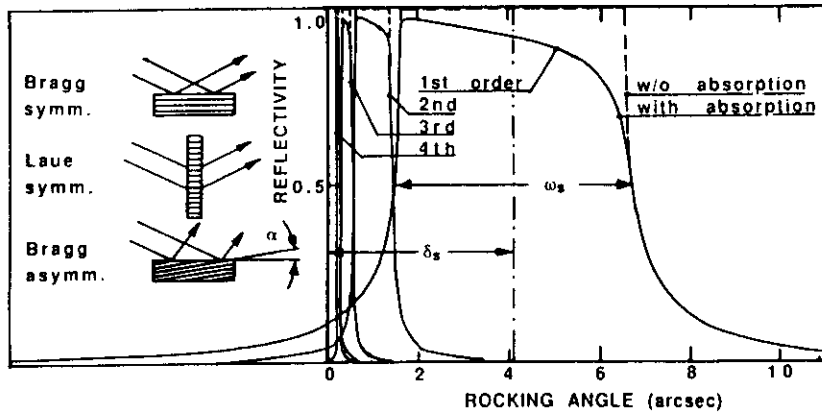


Fig. III.3. Intrinsic perfect crystal diffraction profiles (Si (2n,2n,0)) for a first order wavelength of 1.54 Å.

The variation of both peak width and position as a function of reflection order is also seen in Fig. III.3. The reflection pattern  $r(\Delta)$  corresponds to the reflected intensity, normalized to the incident intensity of a monochromatic and parallel X-ray beam. Recorded as a function of the angle it is often called "rocking curve" and has the following shape:

$$r(\Delta) = L - (L^2 - 1)^{1/2} \quad (\text{III.12})$$

where  $L$  depends in a complicated way on the crystal structure factor, absorption, polarization and other parameters.

The width of the rocking curve (Darwin width) for the symmetric case is given by

$$\omega_s = 2(\lambda^2 r_0 C |F_{hr}| e^{-M}) / (\pi v_0 \sin 2\theta_b) \quad (\text{III.13})$$

where  $r_0$  is the classical electron radius,  $C$  is the polarization factor ( $= 1$  for  $\sigma$ -polarization and  $\cos 2\theta_b$  for  $\pi$ -polarization),  $F_{hr}$  is the real part of the structure factor,  $e^{-M}$  is the Debye-Waller factor and  $v_0$  is the volume of the crystallographic unit cell. This equation can be written as

$$\omega_s = \epsilon_s \tan \theta_b \quad (\text{III.14})$$

with

$$\epsilon_s = 4(d_h^2 r_0 C |F_{hr}| e^{-M}) / \pi v_0 \quad (\text{III.15})$$

The relative wavelength resolution of a perfect crystal put in a white incident beam of divergence  $\psi_0$  ("white" means an energy bandwidth wider than that accepted by the crystal) can be obtained by differentiating Bragg's law and assuming Gaussian distribution functions when convoluting  $r(\Delta)$  and  $I(\psi)$  as

$$\Delta E/E = (\Delta\lambda/\lambda) = (\omega_s^2 + \psi_0^2)^{1/2} \cot \theta_b \quad (\text{III.16})$$

By comparing Eqs. (III.14) and (III.16) we see that  $\epsilon_s$  is the intrinsic crystal energy resolution that is to first order independent of energy (Bragg case only!) but varies with the square of the  $d$ -spacing and is proportional to the structure factor that in turn depends on  $(\sin \theta)/\lambda = 1/2d_h$ . The extinction thickness, i.e. the penetration depth  $t_c$  perpendicular to the lattice planes is given by

$$t_c = v_0 / (2d_h r_0 C |F_{hr}|) \quad (\text{III.17})$$

so that  $\epsilon_s = t_c/d_h = 2/\pi N_p$  where  $N_p$  is the number of lattice planes participating in the diffraction process. It is related to the Pendellösung length:  $\Lambda = \pi t_c$  (Ch. VI).

If the reflection is asymmetric meaning that the lattice planes make an angle  $\alpha$  with the crystal surface as shown in the insert in Fig. III.3, the width becomes

$$\omega_0 = \omega_s/b^{1/2} \quad (\text{III.18})$$

$$\omega_h = \omega_s \cdot b^{1/2} \quad (\text{III.19})$$

for the incident and exit beams, respectively, where

$$b = \{\sin(\theta_b - \alpha)\} / \{\sin(\theta_b + \alpha)\} \quad (\text{III.20})$$

is the asymmetry factor. The energy resolution and the extinction depth have to be changed accordingly. Associated with the angular beam transformation is the change in spatial cross section of the beam:

$$w_h = w_0/b \quad (\text{III.21})$$

so that

$$\omega_h w_h = \omega_0 w_0 \quad (\text{III.22})$$

which expresses Liouville's theorem. The angular shift of the Bragg peak is given for the symmetric Bragg case by

$$\delta_s = \omega_s F_{or} / (2C |F_{hr}| e^{-M}) \quad (\text{III.23})$$

where  $F_{or}$  is the real part of the structure factor in forward direction. For the asymmetric case one obtains

$$\delta_0 = (1 + 1/b) \delta_s / 2 \quad (\text{III.24})$$

$$\delta_h = (1 + b) \delta_s / 2 \quad (\text{III.25})$$

for the incident and exit beams, respectively.

Both the Darwin width and the shift of the Bragg peak diverge for zero and  $\pi/2$  Bragg angles because the formulae given above correspond to approximations. Exact theories exist also for these extreme cases and have been experimentally verified. Table 2 gives some relevant quantities for two commonly used materials, Si and Ge, and for Be and diamond that have recently become of great importance because of their low X-ray absorption and the very good thermal properties of diamond (see section III.7).

Material (h k l)	$d_h$ [Å]	$r_0 F_{hr} e^{-M} / v_0$ [ $10^{-14}$ cm]	$\omega_s$ [ $\mu$ rad]	$\epsilon_s$ [ $10^{-6}$ ]	$t_c$ [ $\mu$ m]	$t_a$ [ $\mu$ m]
Be (002)	1.7916	5.59	10.7	22.8	5.0	1200
Be (110)	1.1428	4.27	6.49	7.1	10.3	1874
C (111)	2.0589	10.7	23.3	57.8	2.27	250
C (220)	1.2609	9.85	15.4	19.9	4.03	408
Si (111)	3.1355	10.43	34.5	136	1.53	8.7
Si (220)	1.9201	11.45	23.5	53.7	2.27	14.2
Ge (111)	3.2664	22.64	74.8	308	0.68	2.94
Ge (220)	2.0002	26.98	57.2	137	0.93	4.79

Table 2.- Some crystal reflection data for Be, diamond, Si and Ge monochromator crystals and an X-ray wavelength of 1.54 Å ( $E = 8.05$  keV). For symbols, see text.

Si and Ge can be obtained as highly perfect crystals that define their lattice spacing and orientation to within  $10^{-6}$ . This has been shown experimentally. Diamond is less perfect but the deformations produced by growth defects can be as small as 5  $\mu$ rad. On the other hand, Be is a so-called mosaic crystal where the effect of defects is commonly described in terms of an angular distribution of small perfect domains (mosaic blocks) inside the crystal that both give rise to a broadening of the rocking curve. The best presently available Be crystals have a mosaic spread of about 180  $\mu$ rad, their mosaic block size is about a  $\mu$ m. A general problem with mosaic crystals is an often non-uniform mosaic distribution that produces an uneven rocking curve. Therefore, they have to be characterized and selected with care.

The use of two or more reflections from perfect crystals (Si is the most common material), either inside a monolithic block ("channel-cut") or with independent crystals, provides a whole bunch of possibilities for beam conditioning, for example:

- > elimination of higher harmonics by detuning two non-dispersive reflections,
- > high energy and angular resolution in the dispersive mode (see Fig. III.3),
- > high energy and angular resolution by successive asymmetric reflections,
- > cutting the tails by multiple reflections inside a channel cut monolith,
- > high degree of linear polarization by multiple reflections.

For an energy of 8 keV the beam divergence is about 30  $\mu$ rad for undulator sources and ten times higher for bending magnet and wiggler radiation. The best compromise between intensity and energy resolution is often achieved if the white beam divergence equals the rocking curve width of the crystal (see Eq.

III.16). Whereas perfect crystals fulfill this matching condition around 10 keV using also asymmetric reflections, mosaic crystals like Be and annealed Si crystals permit to gain in flux at higher energies if they are not too far from the sample (Freund, 1992). In addition, single crystals can produce or analyze circular polarization. All these applications cannot be described in the framework of this article. Useful information are given by Kohra et al. (1978), Materlik and Kostroun (1978), Hart et al. (1984), Mills (1988), and Ishikawa et al. (1991).

Finally, curved crystals are suitable for focusing, both in meridional and in sagittal direction. Whereas in the second case the energy resolution is not affected, for focusing in the diffraction plane one obtains a specific energy-direction correlation and focusing can be either *monochromatic* if the Rowland condition is fulfilled (Johann and Johansson geometry) or *dispersive* if this is not the case. The same formulae as for mirrors are valid (Eqs. (III.9) and (III.10)) replacing simply  $\theta$  by  $(\theta_b \pm \alpha)$ . The rocking curves are broadened by the crystal deformation and can be calculated from a modified dynamical theory (Gronkowski and Malgrange, 1984). The lower limit of the focal spot size is set by the extinction depth. Reciprocal and phase space diagrams are very useful to show the angle-energy correlation (Suortti and Freund, 1989; Matsushita and Kaminaga, 1980). Special crystal bending devices must be designed and constructed that take into account the very high precision of the deformation required and anticlastic effects in elastically anisotropic materials.

### III.6. Multilayer monochromators

Layered synthetic microstructures are the youngest of all optical devices for hard X-ray instrumentation. Originally, technologies for their fabrication were developed for other purposes, mainly for thin film composite structures for electronic devices. However, during the past two decades specific research and development for VUV and X-ray optical applications increased very rapidly. A convincing demonstration of present and potential applications to X-rays and neutron scattering and of the recent progress in fabrication processes was given in a recent conference organized by SPIE in San Diego (SPIE proceedings Vols. 982, 983 and 984, 1988).

Bragg's law also holds for multilayers and the lattice spacing  $d_{nh}$  has to be replaced by the spacing  $d_1$  of a bilayer. For X-rays, layers of high and low Z should alternate, but this is not the only condition for obtaining good and stable multilayer monochromators. There should be no interdiffusion between the layers, the two materials must be chemically compatible and withstand the high power of synchrotron X-ray beams. My aim here is not to go into detail and also not to describe the advantages and disadvantages of the three major techniques used for multilayer fabrication, which are evaporation, sputtering and molecular beam epitaxy. For the present state-of-the-art, the Symposium Proceedings, Vol. 103, of the Materials Research Society can be consulted. The main problems encountered are interface roughness and variations of layer thickness, which both affect reflectivity and become very important when the d-spacing is decreased which is necessary for monochromators for X-rays of higher energies. At present, d-spacings of bilayers are in the order of 15 Å, and 10 Å or less are envisaged.

Fig. III.4 shows an example of experimental reflection curves obtained at fixed angle as a function of energy (Bilderback et al., 1983). The multilayers consisted of 260 bilayers of W and C spaced by 15 Å ( $t_w = 6.7$  Å;  $t_c = 8.3$  Å) and of 30 bilayers of Mo and C spaced by 56 Å ( $t_{Mo} = 26$  Å;  $t_c = 30$  Å). Although these results are already several years old, they are still representative for the expected hard X-ray efficiencies. These can be very close to the theoretical values for not too many thick layers (Underwood et al., 1988) and by more than a factor two smaller when a bigger number of thinner layers is required. The calculation of the reflectivity and transmission of multilayers is very similar to Darwin's or Ewald's treatments of diffraction by perfect crystals (Spiller, 1988).

The most attractive feature of multilayers is flexibility at their fabrication. They can be grown on curved surfaces to produce focusing elements, their thickness can be graded in-depth and/or laterally, and the constituting materials can be varied over a wide range to achieve optimum performance for a given application. Thus the range from a "supermirror" where the angle of specular reflection is increased by layer coatings of increasing thickness, until Bragg reflectors with adjustable energy resolution is covered, and even higher-order contamination can be avoided by a periodical change of the layer spacing. The same focusing conditions as for mirrors apply. The reflection properties of curved multilayers were recently described by Marshall (1986). Their performance was experimentally demonstrated by Underwood et al. (1988), where spherical multilayers were arranged in Kirkpatrick-Baez geometry to build an X-ray microprobe. A spatial resolution of  $\sim 1$   $\mu\text{m}$  was achieved.

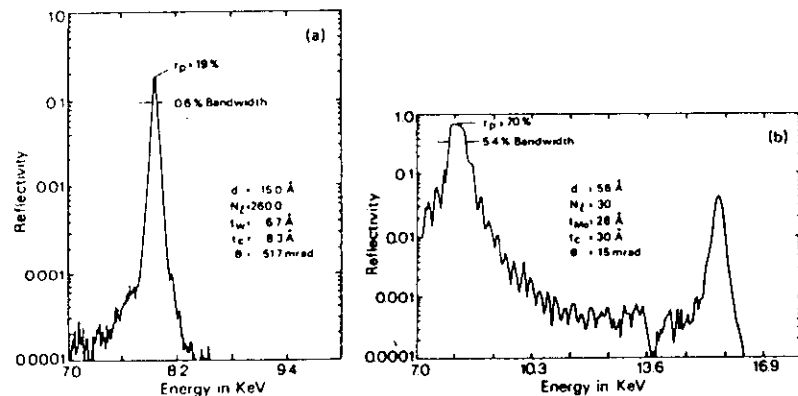


Fig. III.4.- Typical reflectivity profile obtained with multilayers (After Bilderback et al., 1983).

Recently, for very high spatial resolution below 1  $\mu\text{m}$  Bragg-Fresnel Optics was proposed that works even for hard X-ray focusing. This technique is based on a superposition of Bragg diffraction by a single crystal (Aristov et al., 1987; Bonse et al., 1992) or a multilayer (Aristov et al., 1988) and dispersion by a Fresnel structure, either linear or planar, which is grooved into the surface of the Bragg diffracting element. Thus a Bragg-Fresnel element is a multifunctional optical device that permits us to monochromatize, disperse or focus X-ray beams. Its main advantage, however, is that the various possibilities of beam

transformation arising from the specific properties of Fresnel structures now become accessible also to the medium and higher energy X-ray range. Because specular reflection is replaced by Bragg diffraction, the glancing angles are much bigger and efficiency is substantially increased.

### III.7. Thermal problems

Probably the most severe problem that remains to be solved for the efficient use of future high brilliance storage rings is the thermal load produced by very intense photon beams. Already, at existing sources, in particular wigglers, there are problems with cooling the first optical element(s) (beam shapers, crystals, mirrors, windows). Total powers of several kW have to be removed, but the most important difficulty is to reduce the thermal gradients across the surface illuminated by the X-ray beam. These gradients cause internal stresses that deteriorate optical surfaces and produce deformations degrading the spatial and spectral resolution of optical devices. Several methods are used or envisaged to solve the heat load problem: passive cooling by radiation and conduction, active cooling by water or liquid nitrogen, filters based either on reflection or on transmission (absorption), premonochromators (e.g. grazing incidence multilayers) and special designs of monochromators. Their optimum application depends on the type of experiment and on the energy range of interest, and also on the source.

Suitable materials must have high radiation resistance, low thermal expansion,  $\alpha$ , high thermal conductivity,  $\kappa$ , low X-ray absorption,  $\mu$ , so that the figure-of-merit can be defined as  $\kappa/\alpha\mu$ . Table 3 gives these properties for three important monochromator materials. It is seen that for all the thermal properties are strongly improved at low temperatures. At room temperature the best material is diamond but at 125 K the thermal expansion of Si vanishes and the thermal deformation was shown to be below 5  $\mu\text{rad}$  for a power density of 150 W/mm<sup>2</sup> (Freund, 1992a). The problem with diamond for very high resolution is that a big size is not available and that there are some unevenly distributed growth defects. As already mentioned Be crystals are mosaic crystals.

Material	Be	C	Si	Ge
Atomic number, Z	4	6	14	32
Atomic weight, A	9	12	28	73
Lattice constant, a (Å)	2.286	3.567	5.431	5.658
c (Å)	3.583			
Debye temperature, T <sub>D</sub> at R.T., (K)	1188	1860	543	290
Lin. abs. coeff., $\mu$ , at 8 keV (cm <sup>-1</sup> )	1.8	7.5	141	402
Conductivity, $\kappa$ , at R.T. (Wcm <sup>-1</sup> K <sup>-1</sup> )	1.93	2.3	1.5	0.64
Expansion, $\alpha$ , at R.T. (10 <sup>-6</sup> K <sup>-1</sup> )	7.7	1.18	2.4	5.6
Figure-of-merit, 100 $\kappa/\alpha\mu$ at 297 K:	14	26.0	0.44	0.028
at 77 K:	1111	1200	20	0.66

Table 3.- Comparison of some properties of germanium, silicon, diamond and beryllium.

Cooled premonochromators have become the standard equipment in multiple-crystal fixed-exit monochromators. The crystals are attached, either from the side or from below, to cooled copper supports with good thermal contact (indium foil, liquid metal layer). Another possibility is to drill holes in silicon or to grind channels. The problem here is to make tight, reliable and solid connections of the cooling system without deforming the crystals. Cooling by jets appears to be very efficient. Asymmetric reflection geometries (horizontal and/or vertical) permit a decrease of the power density received by the monochromator crystal. Significant engineering efforts are still needed to ensure all safety, reliability, stability, precision and flexibility at the same time. For the present state-of-the-art the interested reader is referred to Rev. Sci. Instr. 63, 1992 and SPIE Proceedings N° 1739/1740 (1992).

## REFERENCES

- ARISTOV, V.V., BASOV, Yu.A., REDKIN, S.V., SNIGIREV, A.A., and YUNKIN, V.A., 1987, Bragg zone plates for hard X-ray focusing, Nucl. Instr. and Meth. A261: 72.
- ARISTOV, V.V., ERKO, A.I., and MARTYNOV, V.V., 1988, Principles of Bragg-Fresnel multilayer optics, Rev. Phys. Appl. 23: 1623.
- BATTERMAN, B.W., and COLE, H., 1964, Dynamical diffraction of X-rays by perfect crystals, Rev. Mod. Phys. 36: 681.
- BATTERMAN, B.W., and BILDERBACK, D.H., 1991, X-ray monochromators and mirrors, in: Handbook on Synchrotron Radiation, Vol. 3, edited by G. Brown and D.E. Moncton, pp. 105-153, Elsevier.
- BILDERBACK, D.H., LAIRSON, B.M., BARBEE, T.W., Jr., ICE, G.E., and SPARKS, C.J., 1983, Design of doubly focusing, tunable (5-30 keV), wide bandpass optics made from layered synthetic microstructures, Nucl. Instr. and Meth. 208: 251.
- BONSE, U., RIEKEL, C. and SNIGIREV, A.A., 1992, Kirkpatrick-Baez microprobe on the basis of two linear single crystal Bragg-Fresnel lenses, Rev. Sci. Instrum. 63: 622-624.
- BORN, M., and WOLF, E., 1964, Principles of Optics, Pergamon Press London.
- CACIUFFO, R., MELONE, S., RUSTICHELLI, F., and BOEUF, A., 1987, Monochromators for X-ray synchrotron radiation, Phys. Rep. 152: 1.
- CHUKHOVSKII, F.N., KRISCH, M. and FREUND, A.K., 1992, Nondispersive Bragg diffraction in the general case of two cylindrically bent crystals, Rev. Sci. Instrum. 63: 920.
- DAVIS, T.J., 1990, DuMond diagram mapping for multi asymmetric crystal monochromators, J. X-Ray Sci. Tech. 2: 180-194.
- DUMOND, J.W.M., 1937, Phys. Rev. 52: 872.
- FREUND, A.K., 1983, On the use of focusing for small-angle scattering experiments, Nucl. Instr. and Meth. 216: 269.
- FREUND, A.K., 1989, X-ray Optics for Synchrotron Radiation, in: Synchrotron Radiation in Structural Biology, Plenum, New York, pp. 255-292.
- FREUND, A.K., 1992a, X-ray optics for ESRF beamlines: problems and projects, Rev. Sci. Instrum. 63: 413-418.
- FREUND, A.K., 1992b, Applications of mosaic crystals to high brilliance X-ray optics, SPIE Proceedings Vol. 1740, paper 07.
- FREUND, A.K., DE BERGÉVIN, F., MAROT, G., RIEKEL, C., SUSINI, J., ZHANG, L., and ZIEGLER, E., 1990, X-ray mirrors for the ESRF, Opt. Eng. 29: 928.
- GRONKOWSKI, J. and MALGRANGE, C., 1984, Propagation of X-ray beams in distorted crystals (Bragg case), Acta Cryst. A 40: 507.
- ISHIKAWA, T., HIRANO, K. and KIKUTA, S., 1991, Complete determination of polarization state in the hard X-ray region, J. Appl. Cryst. 24: 982-986.
- International Tables for X-Ray Crystallography, 1968, Vol. III, pp. 79-87.
- HART, M., and RODRIGUES, A.R.D., 1978, Harmonic-free single-crystal monochromators for neutrons and X-rays, J. Appl. Cryst. 11: 248.
- HART, M., and RODRIGUES, A.R.D., 1979, Tuneable polarizers for X-rays and neutrons, Phil. Mag. B40: 149.
- HART, M., RODRIGUES, A.R.D., and SIDONS, D.P., 1984, Adjustable resolution Bragg reflection systems, Acta Cryst. A40: 502.
- KOHRA, K., ANDO, M., MATSUSHITA, T. and HASHIZUME, H., 1978, Design of high resolution X-ray optical system using dynamical diffraction for synchrotron radiation, Nucl. Instr. and Meth. 152: 161.
- KRISCH, M., 1992, PhD Thesis, ESRF and University of Dortmund, in preparation.
- MALGRANGE, C., 1992, X-ray optics for synchrotron radiation, Acta Phys. Pol. A82: 13-32.
- MARSHALL, G.F., 1986, Monochromatization by multilayered optics on a cylindrical reflector and on an ellipsoidal focusing ring, Opt. Eng. 25: 922.
- MATERLIK, G. and KOSTROUN, V.O., 1980, Monolithic crystal monochromators for synchrotron radiation with order sorting and polarizing properties, Rev. Sci. Instr. 51: 86.
- MATSUSHITA, T., and HASHIZUME, H., 1983, X-ray monochromators, in: Handbook on Synchrotron Radiation Vol. 1, E.E. Koch, ed., 261, North-Holland, Amsterdam.
- MATSUSHITA, T., and KAMINAGA, U., 1980, A systematic method of estimating the performance of X-ray optical systems for synchrotron radiation I and II, J. Appl. Cryst. 13: 465, 472.
- MILLS, D.M., 1988, Phase-plate performance for the production of circularly polarized X-rays, Nucl. Instr. and Meth. A266: 531.
- PARRAT, L.G., 1954, Surface studies of solids by total reflection of X-rays, Phys. Rev. 95: 359.
- SPILLER, E., 1988, Characterization of multilayered coatings by X-ray reflection, Rev. Phys. Appl. 23: 1687.
- SUORTTI, P., and FREUND, A.K., 1989, On the phase space description of synchrotron X-ray beams, Rev. Sci. Instrum. 60: 2579-2585.
- SANCHEZ DEL RÍO, M. and MARCELLI, A., 1992, Waviness effects in ray-tracing of "real" optical surfaces, Nucl. Instrum. Meth. Phys. Res. A319: 170-177.
- SUSINI, J., FÖRSTNER, G., ZHANG, L., BOYER, C. and RAVELET, R., Optimization and theoretical performance of an adaptive X-ray mirror, Rev. Sci. Instrum. 63: 423-427.
- SUSINI, J., 1992, X-ray mirrors for high-brilliance synchrotron beamlines: research and development at ESRF, SPIE Proceedings, Vol. 1740, paper 06.
- UNDERWOOD, J.H. THOMPSON, A.C., WU, Y., and GIAUQUE, R.D., 1988, X-ray microprobe using multilayer mirrors, Nucl. Instr. and Meth. A266: 296.
- WULFF, M., 1992, The optimization of mirror focusing of synchrotron X-ray sources: a test case at the ESRF, SPIE Proceedings Vol. 1740.
- ZACHARIASEN, W.H., 1945, Theory of X-ray Diffraction in Crystals, Dover, New York.